Atomistic Picture of Fluorescent Probes with Hydrocarbon Tails in Lipid Bilayer Membranes: An Investigation of Selective Affinities and Fluorescent Anisotropies in Different Environmental Phases

KNIPPENBERG, Stefan; Fabre, G.; Osella, S.; Di Meo, F.; Paloncyova, M.; AMELOOT, Marcel & Trouillas, P. (2018) Atomistic Picture of Fluorescent Probes with Hydrocarbon Tails in Lipid Bilayer Membranes: An Investigation of Selective Affinities and Fluorescent Anisotropies in Different Environmental Phases. In: LANGMUIR, 34(30), p. 9072-9084.

DOI: 10.1021/acs.langmuir.8b01164
Handle: http://hdl.handle.net/1942/28054

Atomistic picture of fluorescent probes with hydrocarbon tails in lipid bilayer membranes: an investigation of selective affinities and fluorescent anisotropies in different environmental phases

S. Knippenberg[1,2,*], G. Fabre[3], S. Osella[4], F. Di Meo[5], M. Paloncýová[1], M. Ameloot[2], P. Trouillas[5,6]

[1] Division of Theoretical Chemistry and Biology, KTH Royal Institute of Technology Roslagstullsbacken 15, S-106 91 Stockholm, Sweden

[2] Biomedical Research Institute, Hasselt University, Agoralaan Building C, 3590, Diepenbeek, Belgium

[3] LCSN-EA1069, Faculty of Pharmacy, Limoges University, 2, rue du Dr. Marcland, 87025 Limoges Cedex, France

[4] Centre of New Technologies, University of Warsaw, Banacha 2C, 02-097 Warsaw, Poland

[5] INSERM UMR 1248, Faculty of Pharmacy, Limoges University, 2 rue du Docteur Marcland, 87025 Limoges Cedex, France

[6] Centre of Advanced Technologies and Materials, Faculty of Science, Palacký University, tř. 17 listopadu 12, 771 46 Olomouc, Czech Republic

(*) Corresponding author: sknippen@kth.se

Keywords: modeling, photoselection, molecular mechanics, rotational correlation, confocal microscopy

Abstract

By reverting to spectroscopy, changes in the biological environment of a fluorescent probe can be monitored and the presence of various phases of the surrounding lipid bilayer membranes can be detected. However, it is currently not always clear in which phase the probe resides. The well-known orange 1,1′-dioctadecyl-3,3,3′,3′-tetramethylindodicarbo-cyanine perchlorate (DiI-C18(5)) fluorophore for instance as well as the new, blue BODIPY (4,4-difluoro-4-bora-3a,4a-diaza-s-indacene) derivative were experimentally seen to target and highlight identical parts of giant unilamellar vesicles of various compositions, comprising mixtures of dipalmitoylphosphatidylcholine (DPPC), dioleoylphosphatidylcholine (DOPC), sphingomyelin (SM) and cholesterol (Chol). However, it was not clear which of the coexisting membrane phases were visualized (Bacalum *et al.*, Langmuir 32 (2016), 3495). The present study addresses this issue by utilizing large-scale molecular dynamics simulations and the z-constraint method, which allows evaluating Gibbs free energy profiles. The current calculations give an indication why, at room temperature, both BODIPY and DiI-C18(5) probes prefer the gel (S_o) phase in DOPC/DPPC (2:3 molar ratio) and the liquid ordered (L_o) phase in DOPC/

SM/Chol (1:2:1 molar ratio) mixtures. This study highlights the important differences in orientation and location and therefore in efficiency between the probes when they are used in fluorescence microscopy to screen various lipid bilayer membrane phases. Dependent on the lipid composition, the angle between the transition state dipole moments of both probes and the normal to the membrane are found to deviate clearly from 90°. It is seen that the DiI-C18(5) probe is located in the headgroup region of the SM:Chol mixture, in close contact with water molecules. A fluorescence anisotropy study indicates also that DiI-C18(5) gives rise to a distinctive behavior in the SM:Chol membrane compared to the other considered membranes. The latter behavior has not been seen for the studied BODIPY probe, which is located deeper in the membrane.

Introduction

Molecular insight into the condition and properties of lipid membranes, which are fundamental components of living cells, is of utmost importance for various areas of biomedical research including drug design, drug pharmacology, or medical diagnosis and prognosis [1–4]. To give only one example of the crucial role of membranes, it has been shown that increased fluidity and polarity of cell membranes correlate with the metastasis in cancer cells [5]. Well-designed membrane-specific probes can picture biological membrane properties by means of optical imaging and suited spectroscopic techniques. Cholesterol (Chol) highly contributes to the structure of the membranes of many mammal cells [6]. For example, in hepatocellular carcinoma, which is the fifth most frequent cancer worldwide, high Chol levels were found to lead to tumor progression and malignancy [7–9]. The specific development of probe molecules which have an expressed affinity for Chol-abundant membrane regions is a particularly relevant and challenging topic. In the current work, computer modeling is used to investigate interactions of optically active probes with various membrane models and to evaluate whether they can identify the spectral fingerprints of specific biological conditions.

Natural membranes can be organized in different phases, with distinction between single-component and multicomponent membranes. For lipid systems of a single type, a gel phase (S_o) membrane is characterized by a high order of lipid packing. The liquid-crystalline or liquid disordered phase (L_d) of the membrane is characterized by a reduced lipid packing and higher diffusion coefficients. In complex lipid systems, Chol promotes phase segregation and gives access to the liquid-ordered state (L_o), a phase which is often also enriched in sphingomyelin

(SM) [10–13]. The different ratios among the lipid components of a membrane are important parameters that determine its phase. Single component membranes made of dioleoylphosphatidylcholine (DOPC), dipalmitoylphosphatidylcholine (DPPC) or distearoylphosphatidylcholine (DSPC) have been extensively studied [12,14,15]. The phase in a single component system depends on the lipid chemical structure and the temperature. DOPC with its transition temperature of -17 °C adopts a liquid phase at room temperature; the DPPC membrane is in the S_o phase at room temperature but adopts the L_d phase above its transition temperature of 41 °C [16]. Two and/or three components membranes have also been evaluated, *e.g.*, made of DOPC/DPPC or DOPC/SM/Chol in studies, which highlighted that different ratios between the components modulate membrane properties [10,17–21]. Considering the number of possible combinations of membrane components, as well as possible lipid segregations, mixtures of phases are expected in biological membranes. The ternary mixtures can be schematically visualized along with their relevant tie lines in temperature dependent triangular diagrams, from which the phase compositions as well as their coexistence can be read [22–24]. There is finally the need of techniques capable of distinguishing and (locally) characterizing these different phases.

One of the most popular dyes to unravel this complex membrane structure is 1,1'-dioctadecyl-3,3,3',3'-tetramethylindodicarbocyanine perchlorate (DiI-C18(5)). It is a dialkyl carbocyanine (see Figure 1), which is amphiphilic due to the positively-charged head chromophore consisting of two indole rings connected by 5-carbon cyanine moiety and the 18-carbon saturated alkyl chains, which are important for the phase-selective partitioning in the membrane [25,26]. DiI-C18(5) exhibits a high extinction coefficient and a high fluorescence quantum yield, and is highly fluorescent and photostable when incorporated into membranes [27]. Fluorescence spectroscopic analyses of the DiI-family have been used to investigate: membrane rotational lipid mobility [28]; membrane potential [27]; membrane fusion [29]; fluorescence resonance energy transfer [30]; phase separation [31]; lipid leaflet transmigration [32]; and the existence of lipid rafts [33]. As the precise location, orientation and lipid/phase selectivity of the dye is often unknown or only partially described, the interpretation of fluorescence lifetime, anisotropy and rotational dynamics may be complex. Gullapalli *et al*. theoretically investigated the properties of two and four DiI-C18(3) probes, which have a cyanine backbone made of 3 carbon atoms, within a DPPC lipid bilayer in its L_d phase at 323 K, safely above the transition temperature [34]. The probes were found below the head group – water interface and report well the rotational and lateral diffusion components of the lipid dynamics. The calculations showed that the dye

causes minor changes at the interface in the ordering of the water dipoles and electrostatic potential.

Recently, the *meso*-amino substituted BODIPY probe 8-[(2-sulfonatoethyl)amino]-4,4-difluoro-3,5-dioctadecyl-4-bora-3*a*,4*a*-diaza-*s*-indacene (BNP, see Figure 1) was synthetized and optically characterized [35]. This probe expresses similar behavior with respect to membranes as DiI-C18(5), but fluoresces in the blue part of the visible spectrum. The BODIPY dyes are known to combine outstanding spectroscopic and (photo)-physical properties, such as bright fluorescence with absorption and emission bands in the visible range, as well as stability toward light and chemicals. In particular, BNP was found to be excitable by either 1 or 2 photons in combination with a high fluorescence quantum yield; this probe was found to preferentially partition in the same lipid phase as DiI-C18(5) [35]. In this experimental work by Bacalum *et al.*, BNP and DiI-C18(5) were studied in a 2:3 mixture of DOPC:DPPC (L_d:S_o phases) and a 1:2:1 mixture of DOPC:SM:Chol (L_d:L_o phases) at room temperature. Although we could expect a tiny contribution of DOPC to the L_o phase, for simplicity it has been further omitted. Li and Cheng observed that the smaller DiI-C18(3) probe preferentially partitioned in the DPPC S_o phase of the DOPC:DPPC binary mixture [36]. With respect to the ternary mixture, Baumgart *et al.* investigated a 50:27:23 ratio (DOPC:SM:Chol), and reported that DiI-C18(3) preferentially partitions in the DOPC L_d phase [17]. Fluorescence microscopy provided insights into the DiI-C18(3) probe embedded in a dozen ternary mixtures [18]. However, neither for the larger DiI-C18(5) probe nor for BNP, the phase partitioning is known for the specific ratio of lipid systems considered in [35].

It is currently a challenge to accurately evaluate optical properties of the probe within various lipid bilayers. This task first requires a correct and comprehensive evaluation of large scale structural features of the molecular assembly made of the probe and the lipid bilayer, which can be obtained by Molecular Dynamics (MD) simulations. For the current work therefore, MD simulations were performed to gain insight into the interactions of specifically both DiI-C18(5) and BNP probes within biological membranes and to understand their phase preference. Attention is paid to their locations and motions within the lipid bilayers and how this impacts on their spectroscopic features. *In silico* membrane models have been constructed in the past and a vast development with increasing accuracy is noted [37–42]. MD calculations have been used to accurately evaluate simultaneously equilibrium positions of xenobiotics in lipid bilayers, their partition and diffusion coefficients at subpicosecond and atomic resolution [43–

[48]. Focusing on the simulation of optically active probes opens the possibility towards the development of non-invasive techniques which provide insights into the impact of surrounding environment in (non) linear and fluorescence spectroscopy [49,50]. Here, MD simulations are used to assess the interaction of both DiI-C18(5) and BNP in four different lipid bilayers and lipid phases. One of them is the DPPC membrane in its Ld phase, which is considered at the same temperature as in the study of Gullapalli *et al.* [34] to enable a direct comparison. The structural and physical-chemical properties of the four lipid bilayer models are discussed in terms of their areas per lipid, order parameters and non-bonding interaction energies. The Gibbs free energy profiles of DiI-C18(5) and BNP are investigated along the *z*-axis of the membrane, which is oriented perpendicular to the membrane surface. The differences between the equilibrium positions and orientations of both probes, and the variations of their transition dipole moments within the various environments are identified as being decisive for the linear and non-linear optical spectra [51,52]. Finally, the fluorescence anisotropy of both probes is modelled and similarities as well as differences in the behavior of DiI-C18(5) and BNP are highlighted.

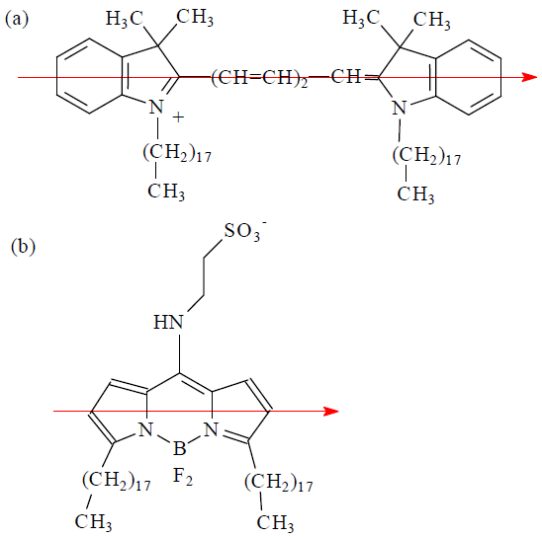

Figure 1: Molecular structures of (a) DiI-C18(5) and (b) BNP. The red arrows are the transition state dipole moments for both probes. To describe the positions of the probes, the middle carbon atom of the –(CH=CH)$_2$–CH= bridge is considered for DiI-C18(5) and the Boron atom for BNP. Remark that the π-conjugated core in both molecules is confined to those parts of the molecules without tails and – in the case of BNP – without headgroup.

Computational details

The MD simulations were performed using the Gromacs 4.5.7 [53,54] software and the Gromos 43A1-S3 force field [55–58]. The lipid bilayer models consisted of 128 lipid molecules

surrounded by at least 4500 explicit water molecules, which were described by the extended single point charge (SPC/E) model. Na^+ and Cl^- ions were added to bulk water at a physiological concentration (0.9%). The spatial reference frame is such that the *x*- and *y*-axes are taken in the plane of the bilayer, whereas the *z*-axis is perpendicular to the membrane surface. Periodic boundary conditions were considered in 3 dimensions. Electrostatic interactions were treated by the particle-Mesh Ewald method [59] and bonds were constrained by the LINCS algorithm [60]. Electrostatics and van der Waals short-range interaction cutoffs were set to 1.6 nm. The NPT ensemble was used, with the Nosé−Hoover thermostat [61,62], and a Parrinello−Rahman barostat [63] for a semi-isotropic pressure coupling at 1 bar and compressibility of 4.5×10^{-5} bar^{-1}. The simulation time step was set to 2 fs and the coordinates in the simulation were saved every 500 steps.

The four lipid bilayer models were built with a homemade script, they consisted out of one probe and in total 128 lipids (two leaflets of 64 lipids): pure DOPC at 298 K (L_d phase), pure DPPC at 298 K (S_o phase) and at 323 K (L_d phase), and a 2:1 SM:Chol mixture at 298 K (L_o phase). The SM acyl chains contain 17 and 15 methyl groups for the sn1 and sn2 acyl chains, respectively. Upon these systems, periodic boundary conditions in all directions have been applied. All membranes were equilibrated during 20 to 40 ns long free simulations, after which convergence of structural parameters (*i.e.*, area per lipid, lipid order parameters…) were ensured. In line with previous work [35], atom types were assigned by PRODRG [64], while partial atomic charges have been used which result from the restrained fit of electrostatic potential (RESP) [65]. They were calculated at the level of density functional theory (DFT) by means of the B3LYP functional [66,67], Dunning's correlation consistent cc-pVDZ basis set [68], and a PCM model which was chosen to describe an implicit solvent model with a dielectric constant of diethyl ether ($\varepsilon = 4.24$) [69]. The Lennard-Jones parameters of the boron atom for the BNP probe, which are not by default present in the applied force field, have been taken from reference [70]. Further parametrizations for the bonded interactions of the Boron atom have been performed by means of previous DFT method.

The Gibbs free energy profiles for BNP and DiI-C18(5) were calculated by means of the *z*-constraint method [71,72], in which bulk water was put as a reference. The distance between the centers of masses of the lipid bilayer and the Boron atom for BNP, or the middle carbon atom of the –(CH=CH)2–CH= bridge for DiI, was constrained, and the required force was monitored.

The averaged force was then used to calculate the Gibbs free energy profile, also called potential of the mean force [72,73], as:

$$\Delta G(z) = -\int_{outside}^{z} \langle F(z') \rangle_t \, dz', \quad (1)$$

where $\langle F(z) \rangle_t$ is the force which is needed to keep the molecule at a given depth *z*. A series of windows was obtained every 0.1 nm for *z*-constraint simulations. The initial structures for each window were generated by merging probe and membrane coordinates, minimized to avoid steric clashes, and *g_membed* [74] was used to remove overlapping lipids when appropriate. In this process, the probes were oriented along the *z*-axis, with the lipid tails in the direction of membrane center. For the *z*-constraint process, 100 ns simulations were performed per window, ensuring convergence of Gibbs free energy profiles. The computational error was found to be ~1 kcal/mol. Starting from the minimum energy positions of the Gibbs free energy profiles, 300 ns long MD simulations were performed without applying additional constraints, of which the first 40 ns were discarded from the simulation window, as being the time required to equilibrate the system. The analysis of the structures of the membranes were performed on these unbiased simulations with GROMACS internal tools, area per lipid for individual lipid types was obtained by the FATSLiM script [75].

The transition state dipole moments of the BNP and DiI-C18(5) probes have been calculated using approximate second order coupled cluster theory (CC2) and the double zeta polarized (DZP) basis set.

In total, these simulations required a computational effort of more than 40 μs. To perform these calculations, the *Lindgren* cluster at the PDC Center for High Performance Computing in Stockholm (864 000 core hours, 2013-2014), the *muk* tier-1 cluster of the Flemish Supercomputer Centre (VSC) (264 960 core hours, 2014-2015), as well as the *Beskow*, *Triolith* and *Abisko* clusters with in total 105 000 core hours/month (2015) were used.

Results and discussion

Characterization of the membranes

If the simulated DOPC (L_d), DPPC (S_o), DPPC (L_d) and SM:Chol (L_o) bilayer membranes are expected to influence the distribution and dynamic behavior of the embedded probes, their inherent properties should be accurately modelled. The structure of lipid membranes can be

well described by the density plots of various membrane components along the normal axis to the membrane plane. The density distributions of the lipid constituents and of water from the center of the membrane were constant between 2 nm and 0.8 nm for SM:Chol (Figure 2). In the other three membranes, locally higher lipid density was found with a peak at around 1.7 nm from the center, followed by a rapid decrease to the center. This effect is explained by the presence of free volumes just beneath the aqueous interface in contact with the polar head group region [34,76,77] and is manifestly seen in the SM:Chol membrane. Concomitantly, the thickness of the SM:Chol membrane was greater, as seen by a shifted point where the density of the water equals that of the lipids (*i.e.*, crossing at 2.5 nm for SM:Chol with respect to 2.3 nm for the L_d-phase DOPC and DPPC, see Figure 2). As expected, a similar increase of the thickness was observed for DPPC (S_o).

The thickness, in terms of distance of the highest density peaks, agrees well with experimental data. We observed differences in thickness between the different membranes, namely 4 and 4.5 nm for the DPPC (L_d) and the SM:Chol bilayer, respectively. The latter simulated thickness agrees with the experimental value of 4.6-4.7 nm [78]. This value mainly depends on SM, as Chol is known not to significantly modify the conformation of SM molecules [14]. The thickness of the DOPC and DPPC (S_o) bilayers is found in between 4 and 4.5 nm.

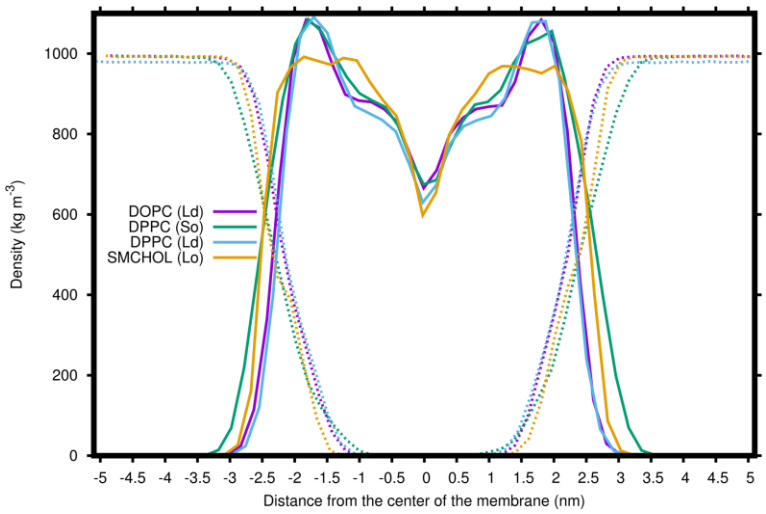

Figure 2: Density distributions of the lipid constituents (full line) and of water (dotted line) within the various membrane phases with respect to the center of the membrane

Over the 300 ns of MD simulations, the area per lipid exhibited constant values, *i.e.*, ~0.45 nm^2/lipid for SM:Chol (L_o, 0.40 nm^2/Chol and 0.48 nm^2/SM), ~0.51-0.52 nm^2/lipid for DPPC (S_o), 0.58 nm^2/lipid for DOPC and DPPC (L_d) (Figure S1). Although the calculated area per

lipid in the L_d phase is lower than some of the reported experimental data [79],],the area/lipid values represent well the differences in the studied phases. A tighter packing and condensing effect were previously observed in S_o phase as well as in the presence of Chol [80].

The potential energy of interaction between the lipid tails (V_{tails}) can be derived from the average sum of Lennard-Jones and short-range Coulomb potentials between all pairs of atoms in the lipid tail region [80,81]. Concerning Chol, all atoms but the hydroxyl group were included, whereas for phospholipids, all tail atoms up to the three glycerol carbon atoms were included. The potential energy was averaged from 180 to 280 ns. The V_{tails} values per atom are very similar for all four membrane models (1.193, 1.127 and 1.110 kcal/mol for DPPC (S_o), SM:Chol and DPPC (L_d), respectively). The decreasing values from 1.193 to 1.110 kcal/mol mainly point the decrease of van der Waals contacts between lipid tails. The latter value is different from that of DOPC, which amounts to 1.182 kcal/mol, likely be due to the greater van der Waals interactions between the unsaturated bonds deep in the DOPC tails not present in the DPPC molecules. Finally, the value for DPPC (S_o) agrees with the one communicated by Wennberg *et al.* in 2012 [80].

To characterize the employed membrane models, the order parameter $|S_{CD}|$ is calculated, too. It is experimentally obtained using deuterium NMR by using the equation [34,82]

$$S_{CD} = \left\langle \frac{3}{2}(\cos^2 \theta_{CD}) - \frac{1}{2} \right\rangle, \quad (2)$$

with θ_{CD} being the angle between C-H bond of the lipid tails and the *z*-axis. The brackets denote time averaging and corresponds to an ensemble averaging when experiments are performed. The value of the order parameter S_{CD} can vary from -0.5 with $\theta_{CD} = 90°$ (indicating full ordering of the C-H bonds perpendicular to the z-axis and to a lesser extent an orientation of the C-C bonds along the *z*-axis) to 1 with $\theta_{CD} = 0°$ (indicating full ordering of the C-H bonds along the *z*-axis and the C-C bonds therefore more oriented perpendicular to the *z*-axis). Based on S_{CD} values, we confirmed the typical differences between the membranes in the L_d, S_o and L_o phases: as reported in Figure S2, $|S_{CD}|$ values for the sn-1 and sn-2 tails amount maximally to ~0.40 for SM:Chol, ~0.35 for DPPC (S_o), and 0.25 for both DOPC and DPPC (L_d). These maxima are obtained at carbon C8 for SM:Chol and DPPC (S_o), while for DOPC and DPPC, the maxima are reached at C6. For C3, close to the headgroup and the glycerol moiety of the lipids, S_{CD} amount to 0.27 for SM:Chol as well as for DPPC (S_o), and to 0.20 for both L_d

membranes. For SM:Chol, the quite strong increase in $|S_{CD}|$ towards the middle of the tail can be linked with the presence of Chol, which pushes the tails of SM deeper in the membrane, so as to accommodate the perpendicular orientation of the C-H bonds, diminishing hydrophobic effects. On the other hand, for DPPC (S_o), the high $|S_{CD}|$ values are related to the high packing, in agreement with V_{tails} values, and with the higher amount of water present at the level of the glycerol group of the tails (Figure 2).

Gibbs free energy profiles for DiI-C18(5)

z-Dependent Gibbs free energy profiles provide information about partition and preferred positions (free-energy minima), as well as capacity of transfer from one to the other leaflet (Gibbs free energy barriers) independently from diffusion effects. The profile for DiI-C18(5) (Figure 3, left hand side) exhibits the deepest well (-38 kcal/mol) in the DPPC (S_o) membrane. The well is energetically less favorable by 5 kcal/mol in both the DPPC (L_d) and SM:Chol (L_o) bilayers; therefore based on the Gibbs free energy alone, one cannot distinguish any preferred affinity to both DPPC (L_d) and SM:Chol (L_o) bilayers. The affinity of DiI-C18(5) to DOPC (L_d) membrane is the least favorable one (potential well of -28 kcal/mol). The here presented data seem to answer therefore the question which membrane DiI-C18(5) prefers in a DOPC:DPPC (L_d:S_o) and a DOPC:SM:Chol (L_d:L_o) mixture, like has been used by Bacalum *et al.* in ref. [35]. Namely, the simulations indicate that in the former case, after equilibration of the biological environment, confocal microscopy will allow visualizing the DPPC (S_o) regions of the unilamellar vesicle, whereas in the latter case, the L_o region of the SM:Chol mixture will be bright. For the concentrations used in the current study, DiI-C18(5) should thus be considered as a L_o marker, and contrasts therefore with the findings of Baumgart *et al.* and Kahya *et al.* for DiI-C18(3) embedded in ternary lipid mixtures with other concentration ratios [17,18].

From the analysis given in Figure 3, the position of the global minima were similar except for SM:Chol (1.3, 1.3, 1.2 and 1.9 nm for DOPC (L_d), DPPC (S_o), DPPC (L_d) and SM:Chol (L_o), respectively). Although in this latter case, the bilayer thickness is greater, this makes DiI-C18(5) closer to the polar group region in SM:Chol with respect to the other membranes.

As we applied the *z*-constraint method from the center of the membrane and used a window for every Ångström, the barriers of transfer from one to the other leaflet have been obtained.

Significant differences are seen: the barrier at the middle of the bilayer is ~8 kcal/mol with DOPC and SM:Chol, and it is lower (4-5 kcal/mol) with DPPC (L_d) and DPPC (S_o). As repeatedly seen with amphiphilic compounds, the insertion into fluid bilayers requires small or even no energetic barriers in the polar head group region. Noncovalent interactions (electrostatic and H-bonding) mainly drive insertion and positioning, with little influence of size within the µs timescale.

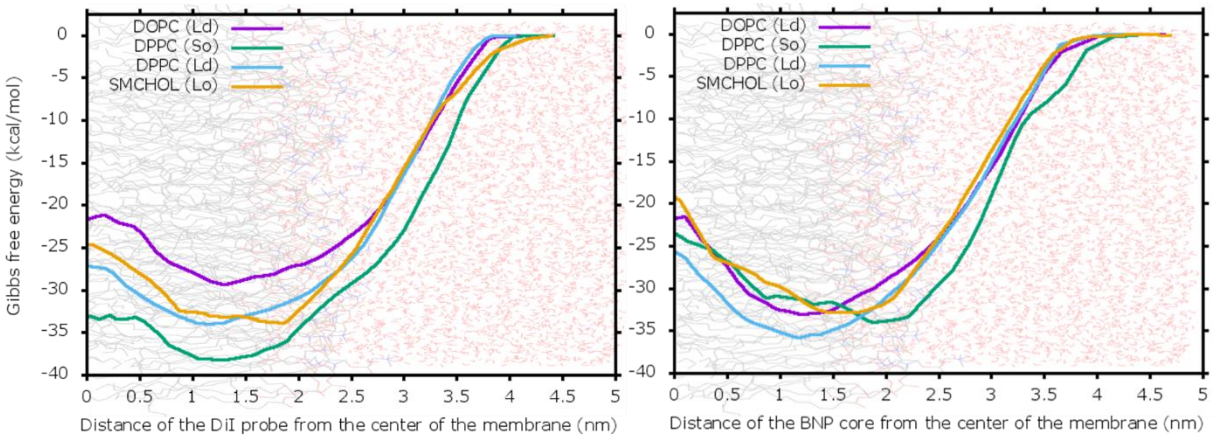

Figure 3: Gibbs free energy surfaces of (left) DiI-C_{18}(5) and (right) BNP in function of the distance (in nm) from the center of the membrane along the *z*-axis, perpendicular to the membrane surface. The centers of mass of the DiI-C18(5) and BNP cores have been constrained. The error bar is contained in the thickness of the line.

Analysis of the unconstrained trajectories for DiI-C18(5) in the various membranes

It is worth noting that the Gibbs free energy profiles are generated based upon a constrained movement of the core of the probe. To discuss the equilibrated positions and orientations of DiI-C18(5) and to profoundly evaluate the influence of the finite temperature, a free production run of 300 ns was performed for each membrane in the presence of DiI-C18(5), with the minima of the Gibbs free energy profile as starting geometries. Illustrations of the DiI-C18(5) probe in the various membranes are given in Figure 4. As a measure for the position of DiI-C18(5), the middle carbon atom of the cyanine-backbone was considered with respect to the membrane center. For SM:Chol, DiI-C18(5) is situated at 1.75±0.11 nm from the membrane center, in close contact to the polar head group region (Figure 5). For both DPPC bilayers, DiI-C18(5) is located deeper, at ~1.0 nm from the membrane center, *i.e.*, in contact with the lipid tails (the exact value for the S_o is 1.04±0.09 nm, while it is 1.09±0.09 nm for the L_d phase). Gullapalli *et al.* observed a value which was with its 1.26 nm a bit higher for DiI-C18(3) in DPPC (S_o) [34]. In DOPC, the location is an intermediate of the other two, however with a broad distribution ranging from 1.3 to 1.8 nm (1.47±0.21). Except for SM:Chol, the mean positions in free

simulations were slightly deeper than the positions of the free energy minima, but these differences were found within errors and thermal motion. In all membranes, the probes have their light sensitive core embedded in lipid head groups and the lipophilic tails pointing towards the center of the membrane. We calculated the angles of the tails of DiI-C18(5) with the *z*-axis (Figure S3). These angles take the value ~155° for both L_d membrane phases, ~165° for DPPC in the S_o phase, and ~170° for SM:Chol in the L_o phase.

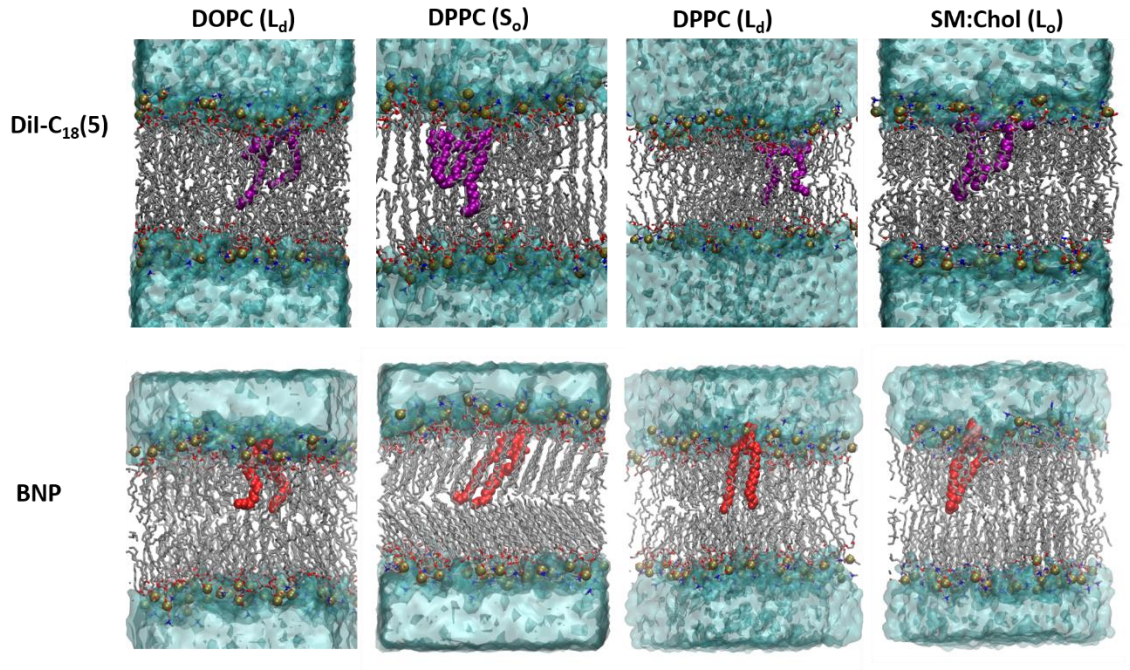

Figure 4: Illustrations of the DiI-C18(5) and BNP probes in the different environments under investigation in the current study.

While in SM:Chol the chromophore moiety of DiI-C18(5) is located at the surface of the membrane in contact with bulk water, it is located significantly more deeply in the other membranes. The DiI-C18(5) π-conjugated core is located below the level of the phosphates at a distance of 0.5 nm in SM:Chol, 0.3-0.8 nm in the L_d phase of DOPC, 1.0 nm in the L_d phase of DPPC and 1.2 nm in So phase (DPPC). In the SM:Chol membrane one has to consider not only the average level of membrane surface, but also a local arrangement of the membrane. The chromophore moiety of DiI-C18(5) experiences here free volumes and induces a small cavity, in which water molecules are pulled (Figure S4). Indeed, due to this surface position and such re-arrangements, DiI-C18(5) is more surrounded by water molecules in the SM:Chol membrane than *e.g.* in the S_o phase or the L_d phases of DPPC. For SM:Chol, at the DiI-C18(5) preferred position, the density of water is still 45% of that of the pure water layer, while practically no water is left with DPPC both in S_o and L_d phases (Figure 2). It can also be remarked that the maximum density of water experienced by DiI-C18(5) in the DOPC (L_d) membrane amounts

to 20%. This effect is quantified by the radial distribution functions of DiI-C18(5) and the surrounding water molecules in the various membranes (Figure S5): the first maxima (at 0.45 nm from the DiI-C18(5) core) is very low for both phases of DPPC membranes (<0.2), slightly higher in DOPC (0.3) and significantly higher in SM:Chol (0.6). The water cavity experienced in the SM:Chol membrane is then responsible for the different behavior of DiI-C18(5) in this membrane.

Being decisive for the photoselection of the probe, the distribution of the angles between the transition dipole moment and the *z*-axis of the membrane is given in Figure 5. For DiI-C18(5), the transition dipole moment is oriented along the cyanine backbone and is displayed in Figure 1. Knowing that a perfect photoselection in confocal microscopy requires an angle of 90°, DiI-C18(5) in DOPC appears the most efficient with a most populated angle of ~85°. For SM:Chol and DPPC (S_o), the most abundant peak is seen at 72°. It can be remarked that for DPPC (S_o), the distribution of the angle is rather symmetric around its maximum, while for SM:Chol a slight asymmetry is seen together with a minor shoulder at higher values. The DPPC (L_d) lipid bilayer is characterized by a broad distribution of angles of a similar population, which are between 70° and 80°, which agrees with the angle of 77° reported for the smaller DiI compounds investigated by Gullapalli *et al.* [34] or with the range of ±10° around the perpendicular position with respect to the z-axis reported by Axelrod for erythrocyte ghosts [83]. The pronounced angles of the transition state dipole moments in the different membranes can be related to the differences in orientation between the sn-1 and sn-2 chains of the lipids and to the differences in position of the probe along the z-axis. To better describe the orientation of DiI-C18(5), the angle between the normal to the coplanar core and the *z*-axis was followed as well. A symmetric distribution was obtained centered at around 51° only for SM:Chol. In DOPC, essentially all values between 30° and 80° were observed, with only a slight preference for 35-40°. For DPPC (L_d), the angle increased from 30° to 80°. In DPPC (S_o), the angle distribution was ranging from 70° to 80°. Combining the analyses for both angles, S_o, and to a less extend L_o, restrain orientation to the probe.

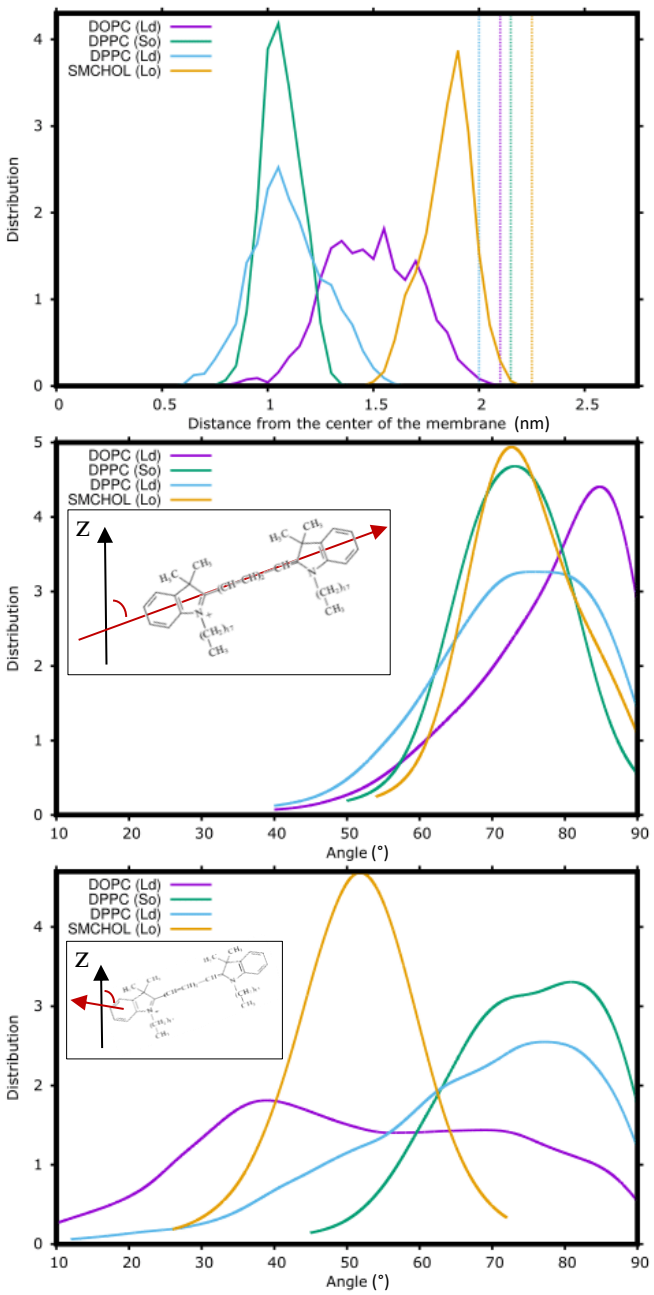

Figure 5: DiI in various membrane phases – (top) the position of the middle atom of the cyanine backbone of DiI along the *z*-axis expressed in terms of the distance from the center of the membrane, the dotted vertical lines denote the most abundant position of the phosphor atoms; (center) the angle between the transition dipole moment and the *z*-axis; (bottom) angle between the axis perpendicular to the plane of the DiI-C18(5) molecule and the *z*-axis. These data are taken from a free MD run and are convoluted with Gaussian profile peaks with a full width half maximum of 8°. The errors are displayed in Figure S6.

The order parameter profiles of DiI-C18(5) show the same trend in all four domains, *i.e.*, higher values close to the polar head group region which decrease when inserting deeper in the bilayer, as expected for lipid-type compounds (Figure 6). Close to the polar head, the highest $|S_{CD}|$ values (0.35-0.39) are observed in SM:Chol (L_o) and DPPC (S_o), whereas lower values (0.20-0.23) are observed in DOPC and DPPC (L_d). A further analysis can be performed making use

of the above definition of S_{CD} which relates to the angles between C-H bonds of the lipid tails and the *z*-axis. Due to the free space which is available at the top of the SM/Chol bilayer and the high abundance of water molecules, the mid C-C bonds of the tails of DiI-C18(5) are seen to straightly enter further down towards the center of the membrane, parallel to the z-axis. In DPPC (S_o), the DiI-C18(5) $|S_{CD}|$ value is also high for the first bonds below the nitrogen atoms, but the curve flattens down and the slope diminishes due to the high packing between the lipid tails, assuring a well-defined and orientation of the last carbon-carbon bonds of the tails. As expected from the position of the probe and the characteristics of the subsequent lipid bilayers, $|S_{CD}|$ values are lower in both L_d-phase membrane models, while the typical decrease along the tails is less steep than for the other two lipid bilayers. In the DOPC membrane, in the middle of the tails of DiI-C18(5), a slight increase of the S_{CD} value is further on observed, which even surpasses the corresponding values for DiI-C18(5) in the DPPC (S_o) environment, which is in DOPC attributed to the double bond.

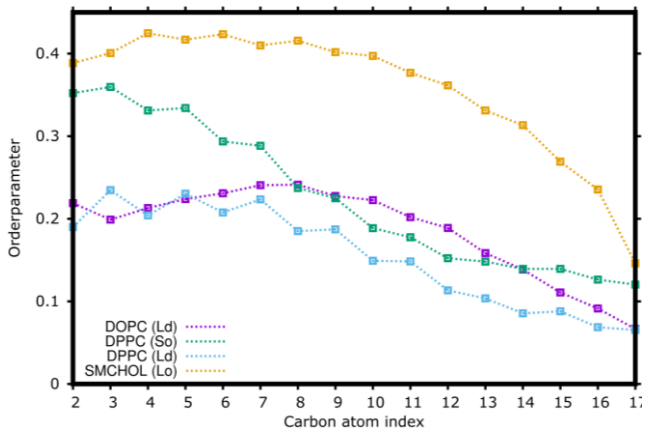

Figure 6: Order parameters for DiI-C18(5) in the various membranes. The carbon atom index points at the number of the carbon in one of the tails, starting from the carbons attached to each of the nitrogens.

Gibbs free energy profiles for BNP

The Gibbs free energy profiles of BNP given in at the right hand side in Figure 3 show a well of -33 kcal/mol in DOPC and SM:Chol; it is marginally deeper in DPPC (S_o) and significantly deeper in DPPC (L_d). Also, the most stable positions of BNP can to some extent be identified within the limits of the used *z*-constraint method. It mostly partitions at 1.2, 1.9, 1.1 and 1.5 nm in DOPC (L_d), DPPC (S_o), DPPC (L_d) and SM:Chol (L_o), respectively. The differences in the preferred position are however less clear than for DiI-C18(5). The markedly small Gibbs free energy differences in these profiles illustrate why within the constraints of the employed theories and simulations a comparison with DiI-C18(5) was needed to identify the lipid phases

present in the bright areas which were seen in the confocal microscopy images published in [35]. Based upon our simulations for DiI-C18(5) and the related discussion above, it is subsequently safe to assume that BNP in the employed biological environments can be found in the S_o phase when a mixture of DOPC (L_d) and DPPC (S_o) is considered and in the L_o phase when a mixture of DOPC (L_d) and SM/Chol (L_o) is involved. We would like to stress here again the importance of the ratio of the employed mixture, as we employed DOPC:SM:Chol in a 1:2:1 ratio. By means of comparison, Baumgart *et al.* reported the L_d phase as the preferred one for the DiI-C18(3) probe in a DOPC/SM/Chol mixture in basically a 2:1:1 ratio [17]. Other authors who reverted to the benchmark DiI-C18(5) probe, discussed the ternary mixtures in other ratios, too, without solving the issue for the mixture under investigation in the current study, but warning for the particular strong influence of the mixed lipid constituents when phase preferences are concerned [18–21].

The barrier for the transfer of BNP between the upper and lower leaflet amounts to ~10 kcal/mol for both DPPC membranes as well as for DOPC. It is calculated as the difference between the minimum of the potential energy surface and the maximum Gibbs free energy value found around the membrane center. The barrier amounts to ~14 kcal/mol for SM:Chol (L_o). The largest differences between both probes are therefore found for DPPC (S_o) and SM:Chol (L_o); the larger barriers are here reported for BNP and should be allocated to the influence of the Boron and Fluorine atoms.

Analysis of the unconstrained trajectories for BNP in the various membranes

As for DiI-C18(5), selecting the frames from the global minima of the Gibbs free energy profiles, a free production run was performed for 300 ns. Illustrations of the BNP probe in the various membranes are given in Figure 4. The boron atom of BNP was at 1.4-1.5 ± 0.2nm from the membrane center in both the DOPC and SM:Chol membranes (Figure 7), while it was inserted deeper (at 1.2 ± 0.2 nm) in DPPC (L_d). Conversely, in DPPC (S_o), it was at ~1.7 ± 0.1 nm, closer to the phosphorus atoms of the membrane surface, being located at 2.25 nm. It can be remarked that the boron atom is located rather close to the lipid tails, while the middle atom of the cyanine backbone of DiI-C18(5) is found higher in the molecule.

This difference in preferred position in the DPPC (S_o) and DPPC (L_d) environments is related to the difference in packing and area per lipid between both membranes. In DPPC (S_o), the packing in between lipid tails is likely to complicate insertion of BNP. Moreover, the core of

BNP has a weak zwitterionic charge distribution between the nitrogen and boron atoms, making them slightly positive and negative, respectively. This favors interactions with water molecules abundant in this region of DPPC (S_o) (up to 20% of the density of pure water). The similar position of BNP in DOPC and SM:Chol is a manifestation of the interaction with tail unsaturation and Chol.

The angle between the transition dipole moment of BNP and the *z*-axis amounts to 70°-75° in DOPC (Figure 7). With an angle of 85° (and a minor distribution at 50°), the photoselection was found to be stronger in DPPC (L_d). In the DPPC (S_o) bilayer, the maximum of the distribution is found at 67°, however a shoulder can also be seen at 86°. Rather in contrast to DiI-C18(5), the angle distribution in SM:Chol is very broad with many contributions between 30° and 60°, and a major peak at 73°.

The orientation of the molecular plane of BNP with respect to the *z*-axis showed that this probe is rather perpendicular to the surface, with an angle of ~85° for DPPC (S_o) and SM:Chol. In DOPC, the maximum is at ~71°, although a shoulder is noticed at 85°. In DPPC (L_d), the distribution is broader, with a shallow maximum at 59°.

Although it has been experimentally found that both DiI-C18(5) and BNP probes target the same membrane phases and in contradiction to the first assumptions [35], it can be concluded based upon the current MD simulations that BNP behaves rather differently from the relatively known DiI-C18(5) one in terms of its orientation and equilibrium position in the membrane.

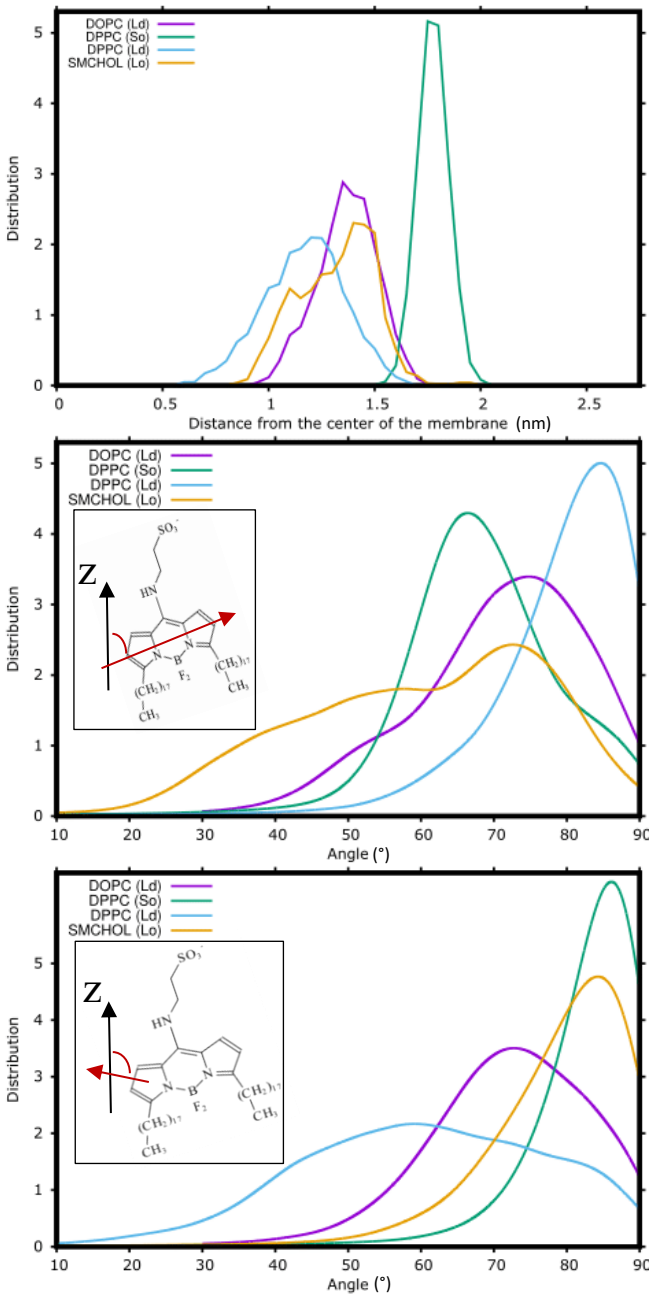

Figure 7: BNP in various membrane phases – (top) the position of the boron atom along the *z*-axis expressed in terms of the distance from the center of the membrane; (center) the angle between the transition dipole moment and the *z*-axis; (bottom) angle between the axis perpendicular to the plane and the *z*-axis. These data are taken from a free MD run and are convoluted with Gaussian profile peaks with a full width half maximum of 8°. The errors for the angle distributions are given in Figure S6.

Fluorescence anisotropy

When polarized light is applied to a biological environment, the probability of excitation of the probe depends on the angle between the transition state dipole moment and the electric field vector of the incoming electromagnetic radiation. A smaller angle leads to a higher excitation

probability. As a consequence, the initial emission after pulsed excitation has a defined polarization. Rotational mobility within a time span determined by the fluorescence lifetime will reduce the fluorescence polarization. The fluorescence anisotropy *r* is generally defined by means of the fluorescence intensities obtained parallel ($I_{//}$) and perpendicular ($I_{\perp}$) to the polarization of the excitation light via

$$r = \frac{I_{//} - I_{\perp}}{I_{//} + 2I_{\perp}}, \tag{3}$$

when the sample is excited with vertically excited light [84].

For DiI-C18(5) and BNP in lipid bilayers of various composition, the relaxation of *r(t)* after a δ-pulse excitation was investigated. This relaxation depends on the rotational dynamics, the intrinsic anisotropy r_0 (corresponding to the anisotropy at t=0) and the conditions of the environment surrounding the light sensitive probe. In agreement with the study by Lipari and Szabo upon the effect of librational motion upon fluorescence depolarization [85] and in line with the theoretical models advocated by Heyn, Jähnig and Ameloot [86–88], the rotational correlation function *C(t)* is an autocorrelation function and is given in terms of the second order Legendre polynomial $P_2(x)=(3x^2-1)/2$ and the orientation of the transition dipole moment at $t = 0$, $\mu(0)$, and time t after excitation, $\mu(t)$ [34,89]:

$$C(t) = \left\langle P_2(\mu(0)\mu(t)) \right\rangle, \tag{4}$$

where the brackets denote the ensemble average, or equivalently, the average over all initial times in the MD calculations, and with $C(t) = \frac{r(t)}{r_0}$ [85]. Since our quantum chemical calculations indicate that the absorption and emission dipoles of the probes under investigation are parallel to each other and as the intrinsic anisotropy r_0 or the anisotropy at time t = 0 for 1-photon excitation depends on the angle δ between both dipoles via [84]:

$$r_0 = \frac{2}{5} P_2(\cos\delta), \tag{5}$$

a maximum value of r_0 = 0.4 has been considered.

Being embedded in a lipid bilayer, the fluorophore has a limited rotational freedom. The fluorescence lifetime (ranging from hundreds of picoseconds to a few nanoseconds) sets a time window over which the rotational motions can be monitored in an experimental context. In line with previous theoretical and experimental analysis [34,35], a double exponential function is used to describe the rotational correlation function:

$$C(t) = \beta_1 \exp(-t/\theta_1) + \beta_2 \exp(-t/\theta_2) + C_\infty , \quad (6)$$

where θ_1 and θ_2 are correlation times. The C_∞ constant reflects that the rotational correlation function, and therefore the fluorescence anisotropy, does not decay to zero. One can define the mean correlation time $\langle\theta\rangle$ as: $\langle\theta\rangle = \frac{\sum_i \beta_i \theta_i^2}{\sum_i \beta_i \theta_i}$.

The results of the analysis are given in Table 1. The quality of the fit was tested by the χ^2 analysis. As our fit leads here to a deviation in the order of barely 10^{-6}, the high quality of the function used is ensured with a time window up to 25 ns. The C_∞ parameter in the S_o phase for both DiI-C18(5) and BNP are the highest ones in the range of investigated environments, pointing at a particularly confined freedom of rotation. The residual C_∞ for both compounds decreases when a more fluid-like lipid environment is considered. It can also be seen that the L_d phase of DPPC displays a slightly smaller constant than the one of DOPC in the same phase. From our analysis, it has been found that C_∞ (S_o) > C_∞ (DOPC, L_d) > C_∞ (DPPC at 323K, L_d) > C_∞ (L_o). These inequalities have to be put in relation to the nature and packing of the various membranes. For the difference between the results for the L_d and L_o phase, the particular position of DiI-C18(5) in the SM:Chol membrane and the presence of the free volumes with water can be recalled. The restricted motions of the probes are finally confirmed by the smaller (larger) relaxation time constants θ_1 (θ_2). For DPPC (L_d) and DiI-C18(3), Gullapalli *et al.* reported θ_1 = 0.99 ns and θ_2 = 6.9 ns for the fast and slow components [34]. These values have to be compared with the ones of 0.11 ns (θ_1) and 11.57 ns (θ_2) found for DiI-C18(5) in this study. The values reported by Ariola *et al.*, who studied DiI-C12(3) in the DOPC (L_d) membrane, can be compared with the ones of Gullapalli *et al.* and amount to θ_1 = 1.2 ns and θ_2 = 9.6 ns [90]. The obtained time constants for the SM:Chol membrane with not only a very low fast component but also a low slow component point at the special place of the DiI-C18(5) probe: a low steric hindrance of the chromophore is seen in the neighborhood of the top of the

lipid acyl chains, while also the collective motion of the lipids in the membrane does not stretch the decay of the rotational autocorrelation function.

A steady-state fluorescence anisotropy of ~0.35 has been measured for BNP in the DPPC S_o phase, while it decreased to ~0.15 upon transition to the L_d phase. The fluorescence lifetimes of this probe reaching up to 4.4 ± 0.2 ns were found to be independent of the phase and the temperature of the lipid system [35]. Especially for BNP, changes in fluorescence anisotropy can consequently be entirely ascribed to restricted tumbling motions of the probe, which are described by Table 1 with the two relaxation times and the limiting anisotropy at long times. From the time constants, it can be seen that the mean relaxation times are larger for BNP than for DiI-C18(5). As the carbocyanines are known to have a shorter fluorescence lifetime of ~1.0 ns [26], the steady state fluorescence anisotropy of BNP is thereupon more sensitive to slower rotational motions than DiI-C18(5). The presented data confirm therefore successfully the assumptions made for BNP at the time of its synthesis [35].

The profoundly low value of 0.12 for C_∞ in SM:Chol as well as the small associated average decay time of 0.43 ns found for DiI-C18(5) point at a strongly pronounced decay of the fluorescence anisotropy and might be another manifestation of the presence of free volumes and a high amount of water molecules in the top polar region of the lipid bilayer. As depicted in Figure 4, the tails of the probe are located along with the acyl tails of the lipids in the membrane. The tails of DiI in SM:Chol are almost parallel to the *z*-axis as can be deduced from the angle of ~170° between the *z*-axis and the vector described by the first and one of the last carbon atoms of the acyl tails of DiI (See Figure S3). Differences between the fitted parameters (*e.g.* C_∞ ~ 0.62 and 0.41 for DiI-C18(5) and BNP in DPPC(L_d) – or 0.12 for DiI-C18(5) and 0.69 for BNP) for DiI-C18(5) and BNP can finally be related to the differences in position of the probes in the lipid bilayer. It is again an indication for the fundamental differences between the two probes. The anisotropy results, together with the Gibbs energy profiles of DiI-C18(5) embedded in the various lipid bilayers, correct and supplement the image for DiI-C18(5) provided in [76] as the probe is not found to perform surface dynamics in the water phase of the membrane but rather tumbles with two relaxation time constants at different distances from the center of the bilayer.

To give an interpretation to the C_∞ parameter, Kinosita *et al.* proposed in 1977 a so-called 'wobbling in a cone' model, in which the transition dipole and the symmetry axis of the probe are assumed to move without restriction in a cone fixed with respect to the membrane [91]. The model relates the C_∞ parameter to half the cone angle such that a large value of C_∞ corresponds to a small cone angle. It can be remarked that the transition state dipole moments for DiI-C18(5) and for BNP are not oriented along the lipid tails of the respective membranes, which invalidates the 'wobbling in a cone' model [85].

When DiI-C18(5) is approximated to a rod which is oriented along the backbone of the probe, Kinosita's other model of 'wobbling outside the cone' could be considered [91], which describes a spatial angle which is avoided by the transition state dipole moment. The analysis of the spherical coordinates (See Figure S7) gives a limited range for the angle between the transition dipole moment and the z-axis, which would be natural for any model describing a wobbling motion, *as well as* for the movement in the plane of the membrane described by the angle φ. It is this hindrance in φ which invalidates the 'wobbling outside the cone' model as it assumes a free movement of the emission dipole moment for this angle. In the figure, it is also seen that the restriction of the motion of DiI-C18(5) in the plane is less severe for the L_d phases than it is for the S_o and L_o phase. These plots are disentangled in Figures S8 and S9, in which the densities for the individual movements along the φ and θ angles are given. All in all, for DOPC(L_d) and DPPC (L_d), the probe can move in the plane of the membrane over angles of 1.4 and 1.2 radians (~80° and ~70°), respectively. For DPPC (S_o) and SM:Chol (L_o), the range of φ amounts to 0.3 and 0.4 radians (~17° and ~22°), respectively. Discarding small artefacts due to a limited simulation time, these plots are found to be symmetric around 0° for φ and 90° for θ. For DiI-C18(5) embedded in SM:Chol, the theta angle is however exclusively restricted to the first quadrant.

Since the tails of the DiI-C18(5) probe can be compared to e.g. the two acyl chains of a DPPC lipid and making abstract of the flexibility of the upper bonds and the out-of-plane distortions of the upper dihedral angles in the tails, the tumbling motion of the backbone and therefore transition state dipole moment of DiI-C18(5) can be related to any wobbling motion of the neighboring lipids. The 3-dimensional movement of the transition state dipole moment is given in Figure 8, showing the specific and restricted movement of the dye up to a timescale of 100 ps. For DPPC (L_d), the movement of the probe can be read and a connection can be made with

the areas of high density in the plane of the molecule, as visualized by the angle φ in Figure S8. The transition dipole moment of the probe describes zones in time with periods of ~60 ns due to a rather constrained movement in phase with the neighboring lipids and exhibits herein a motion with a smaller solid angle. For DOPC, analogous solid areas are seen. For SM:Chol (L_o), the zones are described in ~75 ns, while for DPPC (S_o), this period increases to almost 90 ns.

Table 1 – Pre-exponential parameters β and rotational correlation time θ for DiI-C18(5) and BNP in the four considered environments. All rotational correlation times are given in *ns*.[a]

		β_1	θ_1	β_2	θ_2	C_∞	$\langle\theta\rangle$
DiI-C18(5)	DOPC (L_d)	0.02	0.07	0.09	2.93	0.89	2.91
	DPPC (S_o)	0.02	0.05	0.02	2.67	0.97	2.63
	DPPC (L_d)	0.04	0.11	0.34	11.57	0.62	11.55
	SM:Chol (L_o)	0.47	0.06	0.41	0.48	0.12	0.43
BNP	DOPC (L_d)	0.06	0.39	0.27	24.69	0.65	24.60
	DPPC (S_o)	0.04	0.08	0.03	7.97	0.93	7.83
	DPPC (L_d)	0.11	0.49	0.45	19.31	0.41	19.20
	SM:Chol (L_o)	0.06	0.05	0.25	15.57	0.69	15.56

[a] The mean correlation time $\langle\theta\rangle$ and the C_∞ are also reported.

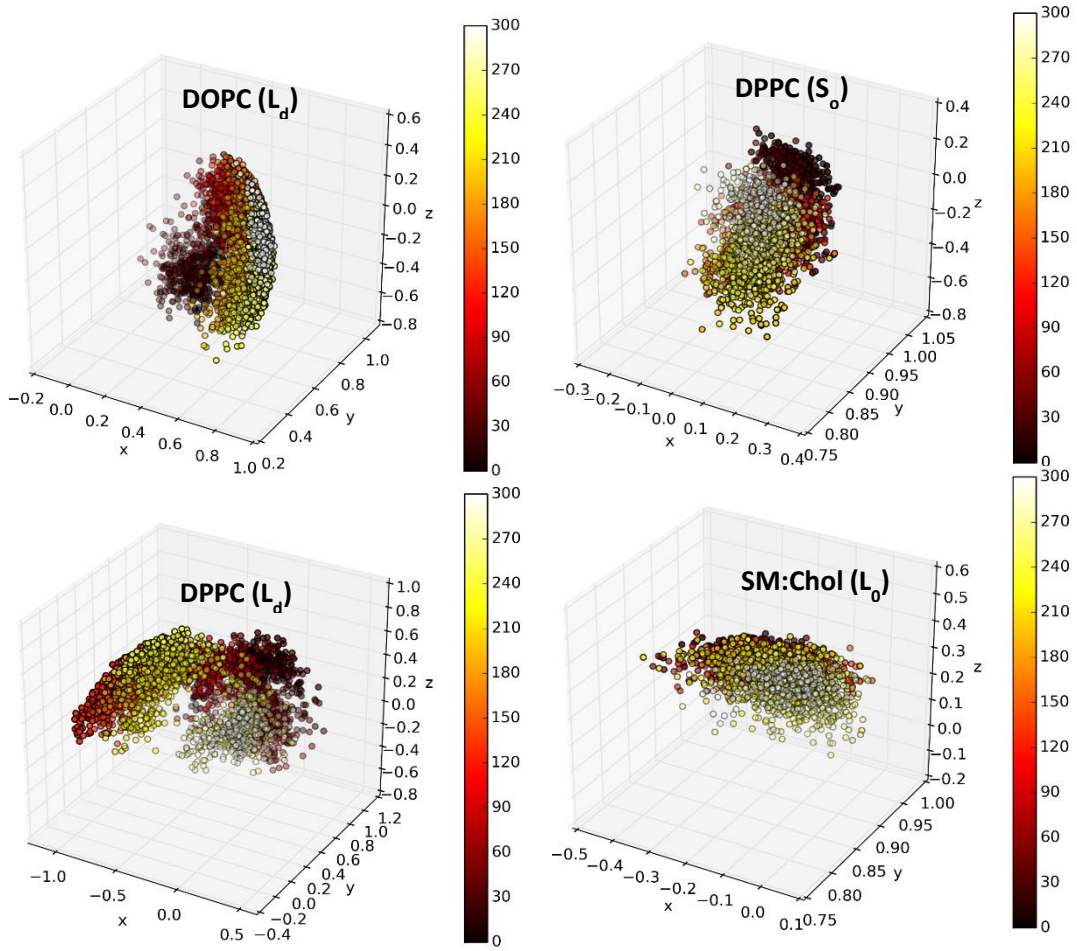

Figure 8: The movement of the transition state dipole moment vector of DiI-C18(5) along the MD trajectory. All vectors have been translated to the origin. One dot corresponds to 100 ps; the time runs from 0 ns (black) to 300 ns (white), as indicated by the color bar.

Conclusions and outlook

The behavior of BNP and DiI-C18(5) molecular probes was investigated in various lipid bilayers in three different phases. By means of demanding MD simulations, the Gibbs free energy profiles of both probes showed that they preferentially partition into the S_o phase of the DPPC bilayer rather than in the L_d phase of the DOPC bilayer. The L_o phase of a 2:1 SM:Chol mixture was also preferred with respect to the L_d phase.

The positions and orientations of the probes are primordial to anticipate their optical properties *in situ*, *e.g.*, in biological membranes. The depths of insertion differ depending on the phase, and that relative to this, the probes in the SM:Chol mixture are stabilized more towards the polar head group region of the membrane. The orientation of the transition dipole moment is

very different with the two probes: for DiI-C18(5), the angle between the transition dipole moment and the *z*-axis in DOPC (L_d) is closer to a perfect 90° value than for the rather new probe BNP. A striking difference is however seen for the molecules in the DPPC (L_d) phase, for which the distribution of the angle ranges from 70° to 80° for DiI-C18(5), while for BNP it peaks at around 85°. From investigations of the membrane density and supported by simulations of the fluorescence anisotropy, it follows that in the SM:Chol (L_o) phase, a high amount of water molecules is found in the vicinity of the probes and that the embedded probes are less restricted in their movement than when they are surrounded by the other membrane phases.

Although the blue fluorescing BNP probe has been introduced as an alternative for the older yellow DiI-C18(5) one, it has been proven that they may behave differently with respect to their interaction with membranes. It is expected that the differences in position and orientation in various biological membranes will affect the linear and more the non-linear absorption spectra. The current research opens therefore a gateway towards a better investigation of the properties of biological membranes and tissues using nonlinear and fluorescent properties of selective molecular probes.

Supplementary information

Area per lipid along the simulated trajectory for the various membranes; order-parameters for the various membrane phases for the sn-1 and sn-2 tails; illustrations of the DiI-C18(5) and BNP probes in the different environments under investigation in the current study; radial distribution functions of DiI-C18(5) and surrounding water molecules for the considered membranes; angle with the *z*-axis of the vector described by the first and fifteenth carbon atom of the acyl tails of DiI; distribution of the vector of the transition dipole moment in spherical coordinates θ and φ; density plots for the vector of the transition dipole moment in function of the azimuthal angle φ; density plots for the vector of the transition dipole moment in function of the angle θ; .itp-files for DiI-C18(5) and BNP.

Acknowledgments

The authors thank the PDC Center for High Performance Computing (local CAC project 1401-002, *Lindgren* cluster), the Flemish Supercomputer Centre (VSC) (Flanders, Belgium) and the Herculesstichting (*muk tier-1* cluster) (Flanders, Belgium), as well as the "Consortium des Équipements de Calcul Intensif" (Céci, with their *Lemaitre2*, *Nic4*, *Hmem*, *Hercules* and *Dragon1* clusters) of the Association Wallonie-Bruxelles for their generous support in terms of computational time. The authors also acknowledge the Swedish SNAC consortium for the medium projects SNIC 2016/1-87 and SNIC 1-415, as well as the small one SNIC 2015/4-44. PT, GF and FDM thank CALI. PT thanks the Czech Science Foundation (P208/12/G016) and National Program of Sustainability I from the Ministry-of-Youth, Education and Sports of the Czech Republic (LO1305). S.O. is grateful to the Center for Quantum Materials and Nordita for his funding in Sweden. S.O. acknowledges the National Science Centre, Poland, grant UMO-2015/19/P/ST4/03636 for the funding from the European Union's Horizon 2020 research and innovation program under the Marie Skłodowska-Curie grant agreement No. 665778. M. P. thanks the Department of Theoretical Chemistry and Biology for her post-doctoral funding at KTH. S. K. is grateful to the Fonds National de la Recherche Scientifique, the French speaking branch of the Belgian National Science foundation, for his postdoctoral funding ('Chargé de Recherches') in Liège. S. K. would also like to thank the group in Limoges for the offered hospitality during his various long term research stays.

References

1 M. A. Lindsay, Target discovery, *Nat. Rev. Drug Discov.*, 2003, **2**, 831–838.
2 I. Green, R. Christison, C. J. Voyce, K. R. Bundell and M. A. Lindsay, Protein transduction domains: are they delivering?, *Trends Pharmacol. Sci.*, 2003, **24**, 213–215.
3 U. Haberkorn, W. Mier, K. Kopka, C. Herold-Mende, A. Altmann and J. Babich, Identification of Ligands and Translation to Clinical Applications, *J. Nucl. Med.*, 2017, **58**, 27S-33S.
4 A. Weiss and P. Nowak-Sliwinska, Current Trends in Multidrug Optimization: An Alley of Future Successful Treatment of Complex Disorders, *SLAS Technol. Transl. Life Sci. Innov.*, 2017, **22**, 254–275.
5 I. Nakazawa and M. Iwaizumi, A Role of the Cancer Cell-Membrane Fluidity in the Cancer Metastases -, *Tohoku J. Exp. Med.*, 1989, **157**, 193–198.
6 D. Voet and J. G. Voet, *Biochemistry*, John Wiley and Sons, Hoboken, NJ, 2011.
7 A. Gorin, L. Gabitova and I. Astsaturov, Regulation of cholesterol biosynthesis and cancer signaling, *Curr. Opin. Pharmacol.*, 2012, **12**, 710–716.
8 A. Fages, T. Duarte-Salles, M. Stepien, P. Ferrari, V. Fedirko, C. Pontoizeau, A. Trichopoulou, K. Aleksandrova, A. Tjonneland, A. Olsen, F. Clavel-Chapelon, M.-C. Boutron-Ruault, G. Severi, R. Kaaks, T. Kuhn, A. Floegel, H. Boeing, P. Lagiou, C. Bamia, D. Trichopoulos, D. Palli, V. Pala, S. Panico, R. Tumino, P. Vineis, H. B. Bueno-

de-Mesquita, P. H. Peeters, E. Weiderpass, A. Agudo, E. Molina-Montes, J. Maria Huerta, E. Ardanaz, M. Dorronsoro, K. Sjoberg, B. Ohlsson, K.-T. Khaw, N. Wareham, R. C. Travis, J. A. Schmidt, A. Cross, M. Gunter, E. Riboli, A. Scalbert, I. Romieu, B. Elena-Herrmann and M. Jenab, Metabolomic profiles of hepatocellular carcinoma in a European prospective cohort, *Bmc Med.*, 2015, **13**, 242.

9 K. Bartel, M. Winzi, M. Ulrich, A. Koeberle, D. Menche, O. Werz, R. Mueller, J. Guck, A. M. Vollmar and K. von Schwarzenberg, V-ATPase inhibition increases cancer cell stiffness and blocks membrane related Ras signaling - a new option for HCC therapy, *Oncotarget*, 2017, **8**, 9476–9487.

10 G. van Meer, D. R. Voelker and G. W. Feigenson, Membrane lipids: where they are and how they behave, *Nat. Rev. Mol. Cell Biol.*, 2008, **9**, 112–124.

11 D. Recktenwald and H. Mcconnell, Phase-Equilibria in Binary-Mixtures of Phosphatidylcholine and Cholesterol, *Biochemistry (Mosc.)*, 1981, **20**, 4505–4510.

12 K. Simons and W. L. C. Vaz, Model systems, lipid rafts, and cell membranes, *Annu. Rev. Biophys. Biomol. Struct.*, 2004, **33**, 269–295.

13 T. P. W. McMullen, R. N. A. H. Lewis and R. N. McElhaney, Cholesterol–phospholipid interactions, the liquid-ordered phase and lipid rafts in model and biological membranes, *Curr. Opin. Colloid Interface Sci.*, 2004, **8**, 459–468.

14 H. Sprong, P. van der Sluijs and G. van Meer, How proteins move lipids and lipids move proteins, *Nat. Rev. Mol. Cell Biol.*, 2001, **2**, 504–513.

15 K. Simons and J. L. Sampaio, Membrane Organization and Lipid Rafts, *Cold Spring Harb. Perspect. Biol.*, 2011, **3**, a004697–a004697.

16 L. K. Buehler, *Cell membranes*, Garland Science, Abingdon, UK, 2016.

17 T. Baumgart, G. Hunt, E. R. Farkas, W. W. Webb and G. W. Feigenson, Fluorescence probe partitioning between Lo/Ld phases in lipid membranes, *Biochim. Biophys. Acta BBA - Biomembr.*, 2007, **1768**, 2182–2194.

18 N. Kahya, D. Scherfeld, K. Bacia, B. Poolman and P. Schwille, Probing Lipid Mobility of Raft-exhibiting Model Membranes by Fluorescence Correlation Spectroscopy, *J. Biol. Chem.*, 2003, **278**, 28109–28115.

19 J. Juhasz, J. H. Davis and F. J. Sharom, Fluorescent probe partitioning in giant unilamellar vesicles of "lipid raft" mixtures, *Biochem. J.*, 2010, **430**, 415–423.

20 K. Bacia, D. Scherfeld, N. Kahya and P. Schwille, Fluorescence Correlation Spectroscopy Relates Rafts in Model and Native Membranes, *Biophys. J.*, 2004, **87**, 1034–1043.

21 D. Scherfeld, N. Kahya and P. Schwille, Lipid dynamics and domain formation in model membranes composed of ternary mixtures of unsaturated and saturated phosphatidylcholines and cholesterol, *Biophys. J.*, 2003, **85**, 3758–3768.

22 R. F. M. de Almeida, A. Fedorov and M. Prieto, Sphingomyelin/phosphatidylcholine/cholesterol phase diagram: Boundaries and composition of lipid rafts, *Biophys. J.*, 2003, **85**, 2406–2416.

23 P. Uppamoochikkal, S. Tristram-Nagle and J. F. Nagle, Orientation of Tie-Lines in the Phase Diagram of DOPC/DPPC/Cholesterol Model Biomembranes, *Langmuir*, 2010, **26**, 17363–17368.

24 N. Bezlyepkina, R. S. Gracia, P. Shchelokovskyy, R. Lipowsky and R. Dimova, Phase Diagram and Tie-Line Determination for the Ternary Mixture DOPC/eSM/Cholesterol, *Biophys. J.*, 2013, **104**, 1456–1464.

25 L. M. Loew, *Spectroscopic Membrane Probes 1*, CRC Press, Boca Raton, Florida, 1988.

26 B. Packard and D. Wolf, Fluorescence Lifetimes of Carbocyanine Lipid Analogs in Phospholipid-Bilayers, *Biochemistry (Mosc.)*, 1985, **24**, 5176–5181.

27 P. J. Sims, A. S. Waggoner, C.-H. Wang and J. F. Hoffman, Mechanism by which cyanine dyes measure membrane potential in red blood cells and phosphatidylcholine vesicles, *Biochemistry (Mosc.)*, 1974, **13**, 3315–3330.
28 B. C. Stevens and T. Ha, Discrete and heterogeneous rotational dynamics of single membrane probe dyes in gel phase supported lipid bilayer, *J. Chem. Phys.*, 2004, **120**, 3030–3039.
29 M. Perin and R. Macdonald, Interactions of Liposomes with Planar Bilayer-Membranes, *J. Membr. Biol.*, 1989, **109**, 221–232.
30 S. Draxler, M. Lippitsch and F. Aussenegg, Long-Range Excitation-Energy Transfer in Langmuir Blodgett Multilayer Systems, *Chem. Phys. Lett.*, 1989, **159**, 231–234.
31 C. Spink, M. Yeager and G. Feigenson, Partitioning Behavior of Indocarbocyanine Probes Between Coexisting Gel and Fluid Phases in Model Membranes, *Biochim. Biophys. Acta*, 1990, **1023**, 25–33.
32 D. Wolf, Determination of the Sidedness of Carbocyanine Dye Labeling of Membranes, *Biochemistry (Mosc.)*, 1985, **24**, 582–586.
33 A. M. Davey, R. P. Walvick, Y. Liu, A. A. Heikal and E. D. Sheets, Membrane order and molecular dynamics associated with IgE receptor cross-linking in mast cells, *Biophys. J.*, 2007, **92**, 343–355.
34 R. R. Gullapalli, M. C. Demirel and P. J. Butler, Molecular dynamics simulations of DiI-C18(3) in a DPPC lipid bilayer, *Phys. Chem. Chem. Phys.*, 2008, **10**, 3548.
35 M. Bacalum, L. Wang, S. Boodts, P. Yuan, V. Leen, N. Smisdom, E. Fron, S. Knippenberg, G. Fabre, P. Trouillas, D. Beljonne, W. Dehaen, N. Boens and M. Ameloot, A Blue-Light-Emitting BODIPY Probe for Lipid Membranes, *Langmuir*, 2016, **32**, 3495–3505.
36 Li and J.-X. Cheng, Coexisting Stripe- and Patch-Shaped Domains in Giant Unilamellar Vesicles †, *Biochemistry (Mosc.)*, 2006, **45**, 11819–11826.
37 D. Bassolinoklimas, H. Alper and T. Stouch, Solute Diffusion in Lipid Bilayer-Membranes - an Atomic-Level Study by Molecular-Dynamics Simulation, *Biochemistry (Mosc.)*, 1993, **32**, 12624–12637.
38 D. Bassolinoklimas, H. Alper and T. Stouch, Mechanism of Solute Diffusion Through Lipid Bilayer-Membranes by Molecular-Dynamics Simulation, *J. Am. Chem. Soc.*, 1995, **117**, 4118–4129.
39 S. J. Marrink and H. J. C. Berendsen, Permeation process of small molecules across lipid membranes studied by molecular dynamics simulations, *J. Phys. Chem.*, 1996, **100**, 16729–16738.
40 R. O. Dror, R. M. Dirks, J. P. Grossman, H. Xu and D. E. Shaw, ed. D. C. Rees, Annual Reviews, Palo Alto, 2012, vol. 41, pp. 429–452.
41 M. Karplus and J. A. McCammon, Molecular dynamics simulations of biomolecules, *Nat. Struct. Biol.*, 2002, **9**, 646–652.
42 M. Karplus and J. Kuriyan, Molecular dynamics and protein function, *Proc. Natl. Acad. Sci. U. S. A.*, 2005, **102**, 6679–6685.
43 T.-X. Xiang and B. D. Anderson, Liposomal drug transport: A molecular perspective from molecular dynamics simulations in lipid bilayers, *Adv. Drug Deliv. Rev.*, 2006, **58**, 1357–1378.
44 D. Bemporad, C. Luttmann and J. W. Essex, Behaviour of small solutes and large drugs in a lipid bilayer from computer simulations, *Biochim. Biophys. Acta-Biomembr.*, 2005, **1718**, 1–21.
45 M. B. Boggara and R. Krishnamoorti, Partitioning of Nonsteroidal Antiinflammatory Drugs in Lipid Membranes: A Molecular Dynamics Simulation Study, *Biophys. J.*, 2010, **98**, 586–595.

46 H. S. Muddana, R. R. Gullapalli, E. Manias and P. J. Butler, Atomistic simulation of lipid and DiI dynamics in membrane bilayers under tension, *Phys. Chem. Chem. Phys.*, 2011, **13**, 1368–1378.
47 M. Paloncyova, K. Berka and M. Otyepka, Convergence of Free Energy Profile of Coumarin in Lipid Bilayer, *J. Chem. Theory Comput.*, 2012, **8**, 1200–1211.
48 N. A. Murugan, R. Apostolov, Z. Rinkevicius, J. Kongsted, E. Lindahl and H. Agren, Association Dynamics and Linear and Nonlinear Optical Properties of an N-Acetylaladanamide Probe in a POPC Membrane, *J. Am. Chem. Soc.*, 2013, **135**, 13590–13597.
49 B. Mennucci, M. Caricato, F. Ingrosso, C. Cappelli, R. Cammi, J. Tomasi, G. Scalmani and M. J. Frisch, How the environment controls absorption and fluorescence spectra of PRODAN: A quantum-mechanical study in homogeneous and heterogeneous media, *J. Phys. Chem. B*, 2008, **112**, 414–423.
50 G. Parisio, A. Marini, A. Biancardi, A. Ferrarini and B. Mennucci, Polarity-Sensitive Fluorescent Probes in Lipid Bilayers: Bridging Spectroscopic Behavior and Microenvironment Properties, *J. Phys. Chem. B*, 2011, **115**, 9980–9989.
51 S. Osella, N. A. Murugan, N. K. Jena and S. Knippenberg, Investigation into Biological Environments through (Non)linear Optics: A Multiscale Study of Laurdan Derivatives, *J. Chem. Theory Comput.*, 2016, **12**, 6169–6181.
52 S. Osella and S. Knippenberg, Triggering On/Off States of Photoswitchable Probes in Biological Environments, *J. Am. Chem. Soc.*, 2017, 4418–4428.
53 D. Van Der Spoel, E. Lindahl, B. Hess, G. Groenhof, A. E. Mark and H. J. C. Berendsen, GROMACS: fast, flexible, and free, *J. Comput. Chem.*, 2005, **26**, 1701–1718.
54 B. Hess, C. Kutzner, D. van der Spoel and E. Lindahl, GROMACS 4: Algorithms for Highly Efficient, Load-Balanced, and Scalable Molecular Simulation, *J. Chem. Theory Comput.*, 2008, **4**, 435–447.
55 S. A. Pandit, S. Vasudevan, S. W. Chiu, R. Jay Mashl, E. Jakobsson and H. L. Scott, Sphingomyelin-Cholesterol Domains in Phospholipid Membranes: Atomistic Simulation, *Biophys. J.*, 2004, **87**, 1092–1100.
56 S. A. Pandit, S.-W. Chiu, E. Jakobsson, A. Grama and H. L. Scott, Cholesterol packing around lipids with saturated and unsaturated chains: a simulation study, *Langmuir ACS J. Surf. Colloids*, 2008, **24**, 6858–6865.
57 S. W. Chiu, S. Vasudevan, E. Jakobsson, R. J. Mashl and H. L. Scott, Structure of sphingomyelin bilayers: a simulation study, *Biophys. J.*, 2003, **85**, 3624–3635.
58 S. A. Pandit, S.-W. Chiu, E. Jakobsson, A. Grama and H. L. Scott, Cholesterol surrogates: a comparison of cholesterol and 16:0 ceramide in POPC bilayers, *Biophys. J.*, 2007, **92**, 920–927.
59 T. Darden, D. York and L. Pedersen, Particle mesh Ewald: An N·log(N) method for Ewald sums in large systems, *J. Chem. Phys.*, 1993, **98**, 10089–10092.
60 B. Hess, H. Bekker, H. J. C. Berendsen and J. Fraaije, LINCS: A linear constraint solver for molecular simulations, *J. Comput. Chem.*, 1997, **18**, 1463–1472.
61 S. Nose, A Unified Formulation of the Constant Temperature Molecular-Dynamics Methods, *J. Chem. Phys.*, 1984, **81**, 511–519.
62 W. G. Hoover, Canonical dynamics: Equilibrium phase-space distributions, *Phys. Rev. A*, 1985, **31**, 1695–1697.
63 M. Parrinello and A. Rahman, Polymorphic Transitions in Single-Crystals - a New Molecular-Dynamics Method, *J. Appl. Phys.*, 1981, **52**, 7182–7190.
64 A. W. Schuttelkopf and D. M. F. van Aalten, PRODRG: a tool for high-throughput crystallography of protein-ligand complexes, *Acta Crystallogr. Sect. -Biol. Crystallogr.*, 2004, **60**, 1355–1363.

65 J. M. Wang, P. Cieplak and P. A. Kollman, How well does a restrained electrostatic potential (RESP) model perform in calculating conformational energies of organic and biological molecules?, *J. Comput. Chem.*, 2000, **21**, 1049–1074.
66 A. D. Becke, Density-functional thermochemistry. III. The role of exact exchange, *J. Chem. Phys.*, 1993, **98**, 5648–5652.
67 C. Lee, W. Yang and R. G. Parr, Development of the Colle-Salvetti correlation-energy formula into a functional of the electron density, *Phys. Rev. B*, 1988, **37**, 785–789.
68 T. Dunning, Gaussian-Basis Sets for Use in Correlated Molecular Calculations .1. the Atoms Boron Through Neon and Hydrogen, *J. Chem. Phys.*, 1989, **90**, 1007–1023.
69 Y. Duan, C. Wu, S. Chowdhury, M. C. Lee, G. M. Xiong, W. Zhang, R. Yang, P. Cieplak, R. Luo, T. Lee, J. Caldwell, J. M. Wang and P. Kollman, A point-charge force field for molecular mechanics simulations of proteins based on condensed-phase quantum mechanical calculations, *J. Comput. Chem.*, 2003, **24**, 1999–2012.
70 E. D. Pietro, G. Cardini and V. Schettino, Ab initio molecular dynamics study of the hydrolysis reaction of diborane, *Phys. Chem. Chem. Phys.*, 2007, **9**, 3857–3863.
71 M. Paloncýová, K. Berka and M. Otyepka, Convergence of free energy profile of coumarin in lipid bilayer, *J. Chem. Theory Comput.*, 2012, **8**, 1200–1211.
72 M. Paloncýová, G. Fabre, R. H. DeVane, P. Trouillas, K. Berka and M. Otyepka, Benchmarking of Force Fields for Molecule–Membrane Interactions, *J. Chem. Theory Comput.*, 2014, **10**, 4143–4151.
73 M. Paloncýová, R. DeVane, B. Murch, K. Berka and M. Otyepka, Amphiphilic Drug-Like Molecules Accumulate in a Membrane below the Head Group Region, *J. Phys. Chem. B*, 2014, **118**, 1030–1039.
74 M. G. Wolf, M. Hoefling, C. Aponte-Santamaría, H. Grubmüller and G. Groenhof, g_membed: Efficient insertion of a membrane protein into an equilibrated lipid bilayer with minimal perturbation, *J. Comput. Chem.*, 2010, **31**, 2169–2174.
75 S. Buchoux, FATSLiM: a fast and robust software to analyze MD simulations of membranes, *Bioinformatics*, 2017, **33**, 133–134.
76 M. M. G. Krishna, A. Srivastava and N. Periasamy, Rotational dynamics of surface probes in lipid vesicles, *Biophys. Chem.*, 2001, **90**, 123–133.
77 S. Lopes and M. Castanho, Does aliphatic chain length influence carbocyanines' orientation in supported lipid multilayers?, *J. Fluoresc.*, 2004, **14**, 281–287.
78 P. R. Maulik and G. G. Shipley, Interactions of N-stearoyl sphingomyelin with cholesterol and dipalmitoyl phosphatidylcholine in bilayer membranes, *Biophys. J.*, 1996, **70**, 2256–2265.
79 D. Poger and A. E. Mark, On the Validation of Molecular Dynamics Simulations of Saturated and cis-Monounsaturated Phosphatidylcholine Lipid Bilayers: A Comparison with Experiment, *J. Chem. Theory Comput.*, 2010, **6**, 325–336.
80 C. L. Wennberg, D. van der Spoel and J. S. Hub, Large Influence of Cholesterol on Solute Partitioning into Lipid Membranes, *J. Am. Chem. Soc.*, 2012, **134**, 5351–5361.
81 F. Di Meo, G. Fabre, K. Berka, T. Ossman, B. Chantemargue, M. Paloncyova, P. Marquet, M. Otyepka and P. Trouillas, In silico pharmacology: Drug membrane partitioning and crossing, *Pharmacol. Res.*, 2016, **111**, 471–486.
82 L. S. Vermeer, B. L. de Groot, V. Reat, A. Milon and J. Czaplicki, Acyl chain order parameter profiles in phospholipid bilayers: computation from molecular dynamics simulations and comparison with H-2 NMR experiments, *Eur. Biophys. J. Biophys. Lett.*, 2007, **36**, 919–931.
83 D. Axelrod, Carbocyanine Dye Orientation in Red-Cell Membrane Studied by Microscopic Fluorescence Polarization, *Biophys. J.*, 1979, **26**, 557–573.
84 Lakowicz, *Principles of Fluorescence Spectroscopy*, Springer, 3rd edition., 2007.

85 G. Lipari and A. Szabo, Effect of Librational Motion on Fluorescence Depolarization and Nuclear Magnetic-Resonance Relaxation in Macromolecules and Membranes, *Biophys. J.*, 1980, **30**, 489–506.
86 M. Heyn, Determination of Lipid Order Parameters and Rotational Correlation Times from Fluorescence Depolarization Experiments, *Febs Lett.*, 1979, **108**, 359–364.
87 F. Jahnig, Structural Order of Lipids and Proteins in Membranes - Evaluation of Fluorescence Anisotropy Data, *Proc. Natl. Acad. Sci. U. S. A.*, 1979, **76**, 6361–6365.
88 M. Ameloot, H. Hendrickx, W. Herreman, H. Pottel, F. Vancauwelaert and W. Vandermeer, Effect of Orientational Order on the Decay of the Fluorescence Anisotropy in Membrane Suspensions - Experimental-Verification on Unilamellar Vesicles and Lipid Alpha-Lactalbumin Complexes, *Biophys. J.*, 1984, **46**, 525–539.
89 W. van der Meer, H. Pottel, W. Herreman, M. Ameloot, H. Hendrickx and H. Schröder, Effect of orientational order on the decay of the fluorescence anisotropy in membrane suspensions, *Biophys J*, 1984, **46**, 515.
90 F. S. Ariola, D. J. Mudaliar, R. P. Walvick and A. A. Heikal, Dynamics imaging of lipid phases and lipid-marker interactions in model biomembranes, *Phys. Chem. Chem. Phys.*, 2006, **8**, 4517.
91 K. Kinosita Jr, S. Kawato and A. Ikegami, A theory of fluorescence polarization decay in membranes., *Biophys. J.*, 1977, **20**, 289.

TOC:

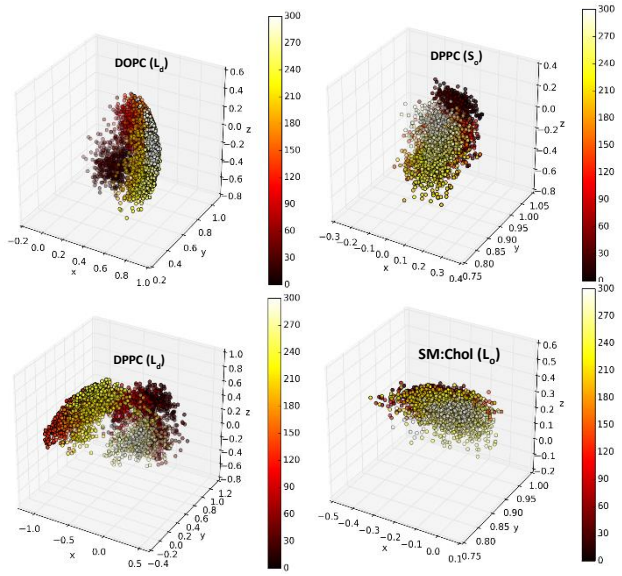

Movement of DiI-C18(5)

Atomistic picture of fluorescent probes with hydrocarbon tails in lipid bilayer membranes: an investigation of selective affinities and fluorescent anisotropies in different environmental phases

Supplementary information

S. Knippenberg[1,2]*, G. Fabre[3], S. Osella[4], F. Di Meo[5], M. Paloncýová[1], M. Ameloot[2], P. Trouillas[5]

[1] Department of Theoretical Chemistry and Biology, KTH Royal Institute of Technology Roslagstullsbacken 15, S-106 91 Stockholm, Sweden

[2] Biomedical Research Institute, Hasselt University, Agoralaan Building C, 3590, Diepenbeek, Belgium

[3] LCSN-EA1069, Faculté de Pharmacie, Université de Limoges, 2, rue du Dr. Marcland, 87025 Limoges Cedex, France

[4] Centre of New Technologies, University of Warsaw, Banacha 2C, 02-097 Warsaw, Poland

[5] INSERM UMR-S850, Faculté de Pharmacie, Université de Limoges, 2 rue du Docteur Marcland, 87025 Limoges Cedex, France

(*) Corresponding author: sknippen@kth.se

CONTENTS

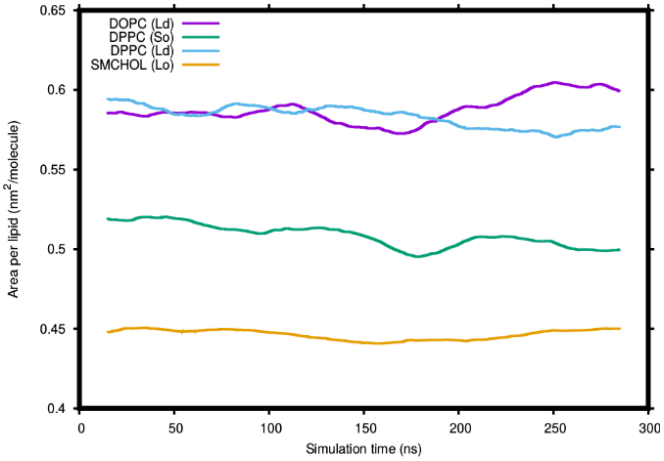

Figure S1: Area per lipid (given in nm^2/molecule) along the simulated trajectory for the various membranes. The moving average is given using 30 terms.

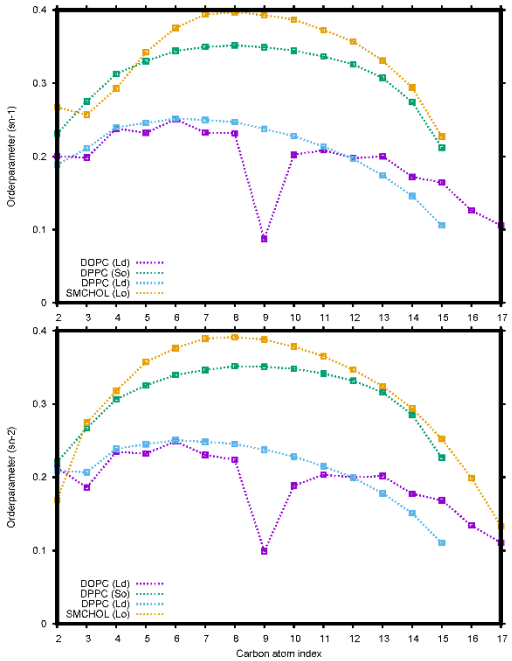

Figure S2: Order-parameters $|S_{cd}|$ for the various membrane phases for the sn-1 tail (top) and the sn-2 tail (bottom). The CH2 groups are numbered consecutively from 2 to the end (18 for DOPC and Sphingomyelin, and 16 for DPPC). Number 1 is the carbonyl carbon. Due to the nature of $|S_{cd}|$, the value for it as well as for the terminal CH_3 group cannot be obtained. The sn-2 tail can be distinguished as it is attached to the middle carbon of the glycerol backbone.

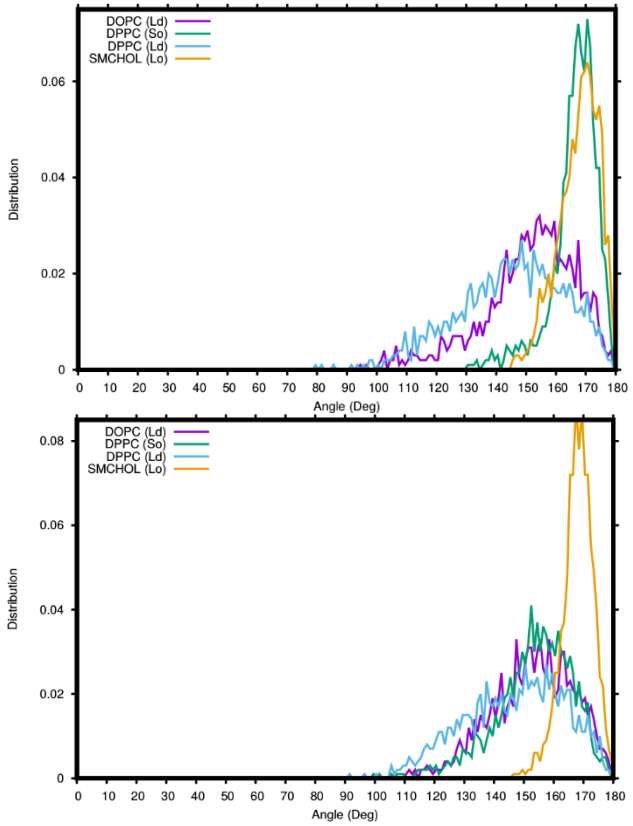

Figure S3: The angle with the *z*-axis of the vector described by the first and fifteenth carbon atom of the acyl tails of DiI. The two tails (top and down part of the figure) are separated out for clarity.

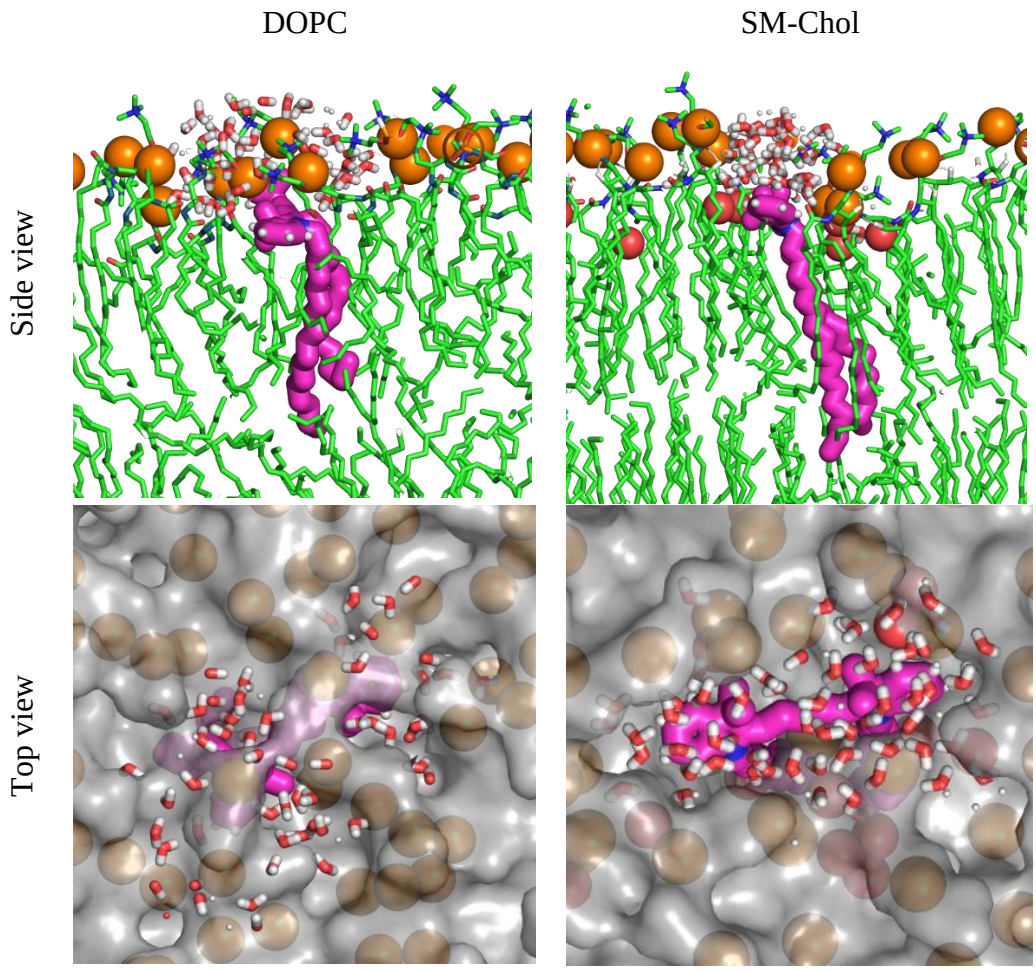

Figure S4: Side view and top view of final frames of free simulation of DiI-C18(5) in DOPC and SM/Chol membranes with highlighted surrounding water molecules. The DiI-C18(5) molecules are shown in magenta sticks, water within 8 Å are shown as red and white sticks, phosphates are displayed as orange balls, oxygen of cholesterol as red balls. In side view, lipid molecules are shown as green sticks (green – carbon, blue – nitrogen, red – oxygen), in top view lipids are displayed as semi-transparent grey surface. In both cases, DiI-C18(5) is in contact with lipid head groups, but in DOPC lipid head groups cover and hinder DiI, in SM/Chol DiI is in direct contact with bulk water and is therefore less hindered by lipid head groups.

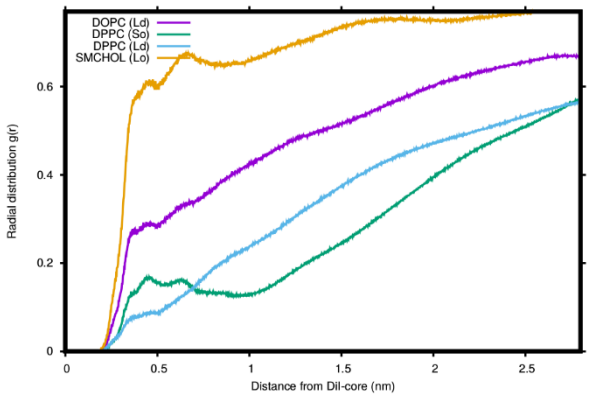

Figure S5: Radial distribution functions of the core of the DiI probe and surrounding water molecules for the various membrane phases.

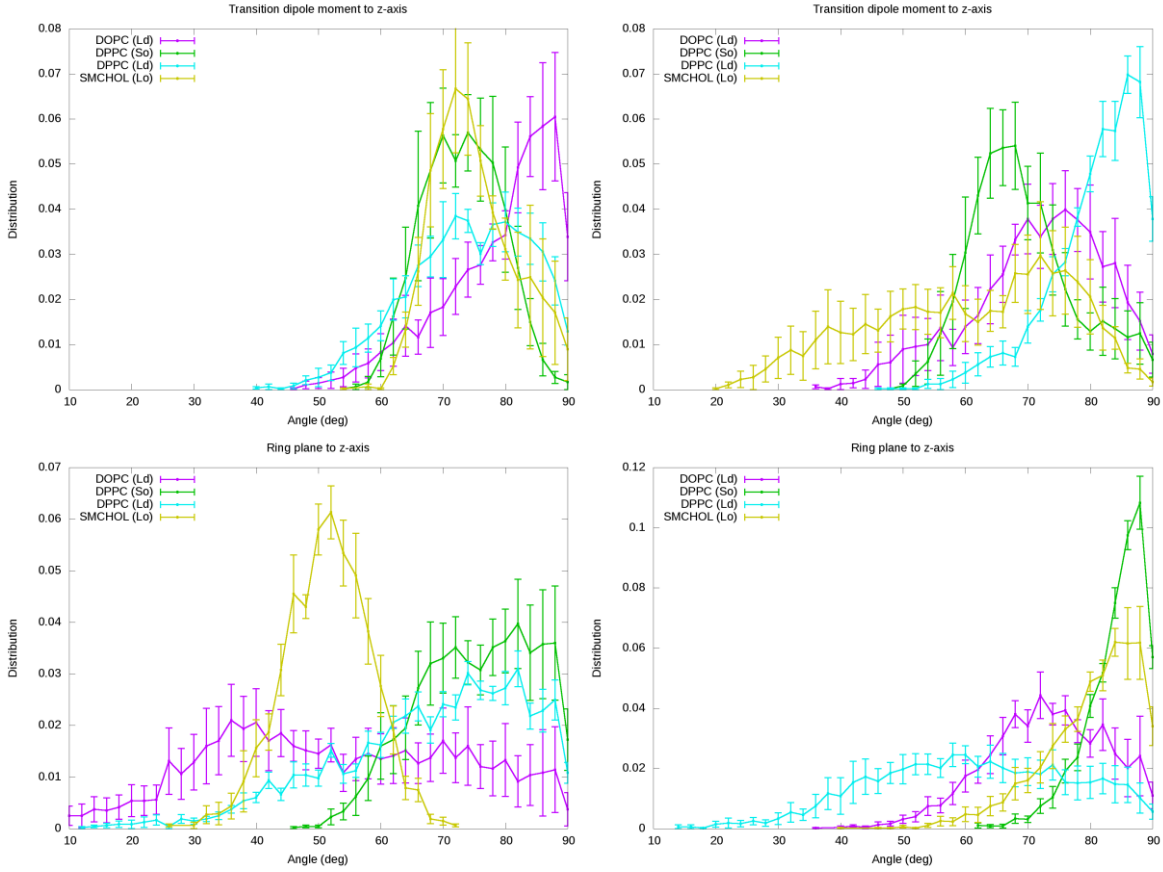

Figure S6: Top: Distribution of the angle between the transition dipole moment and the z-axis in various membrane phases; Bottom: angle between the axis perpendicular to the plane of the DiI-C18(5) (left) or BNP (right) molecule and the z-axis. Smoothed and rescaled plots are displayed in Figures 5 and 7. To obtain the error bars, the distribution plots were calculated for every 40 ns of simulations with bins of 2° (discarding the first 40 ns of the simulations). For each bin, the average and standard error were calculated.

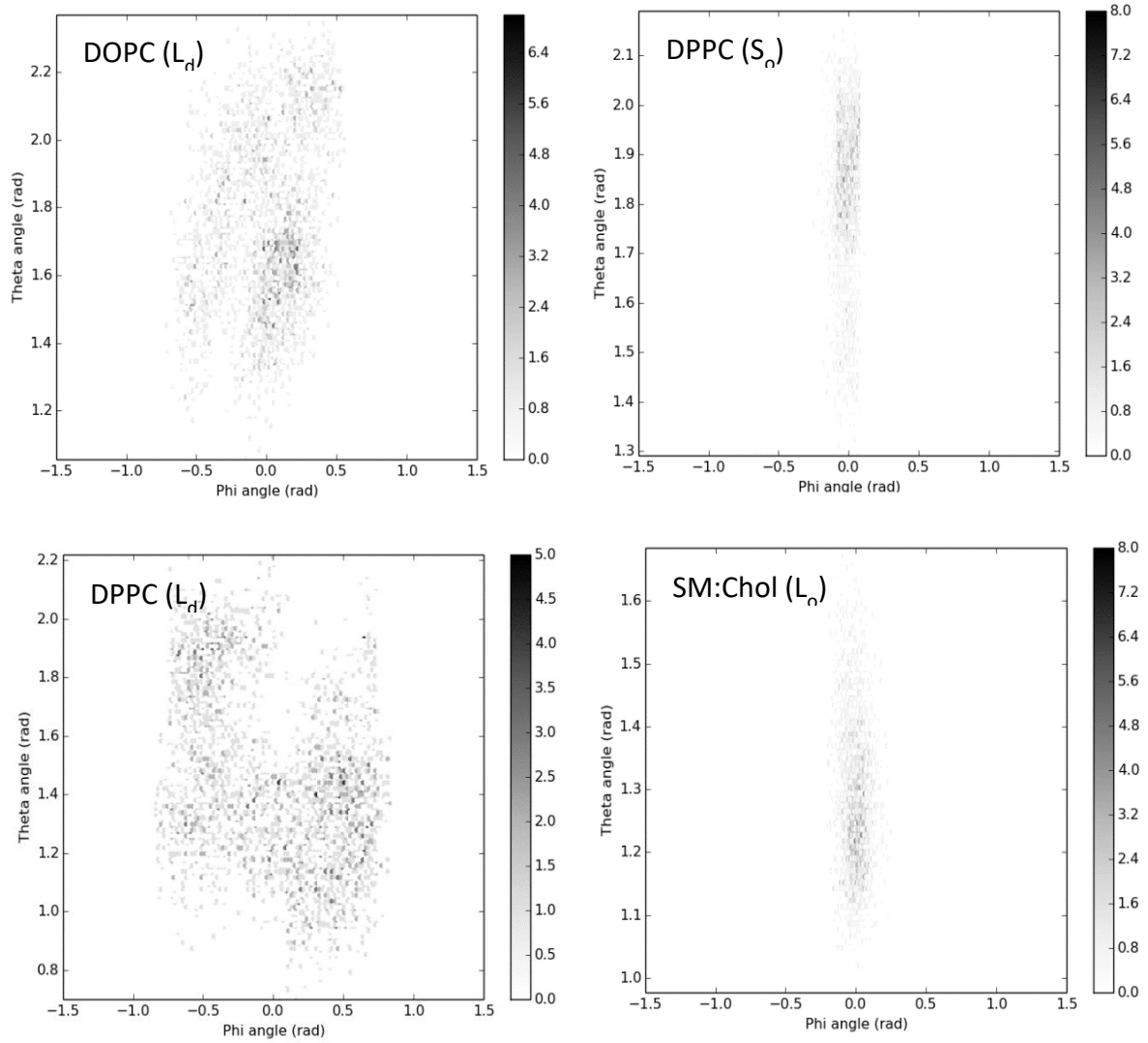

Figure S7: Distribution of the vector of the transition dipole moment in spherical coordinates θ and φ for the four membranes. θ is the angle with the z-axis of the membrane, while φ denotes the angle in the plane of the membrane.

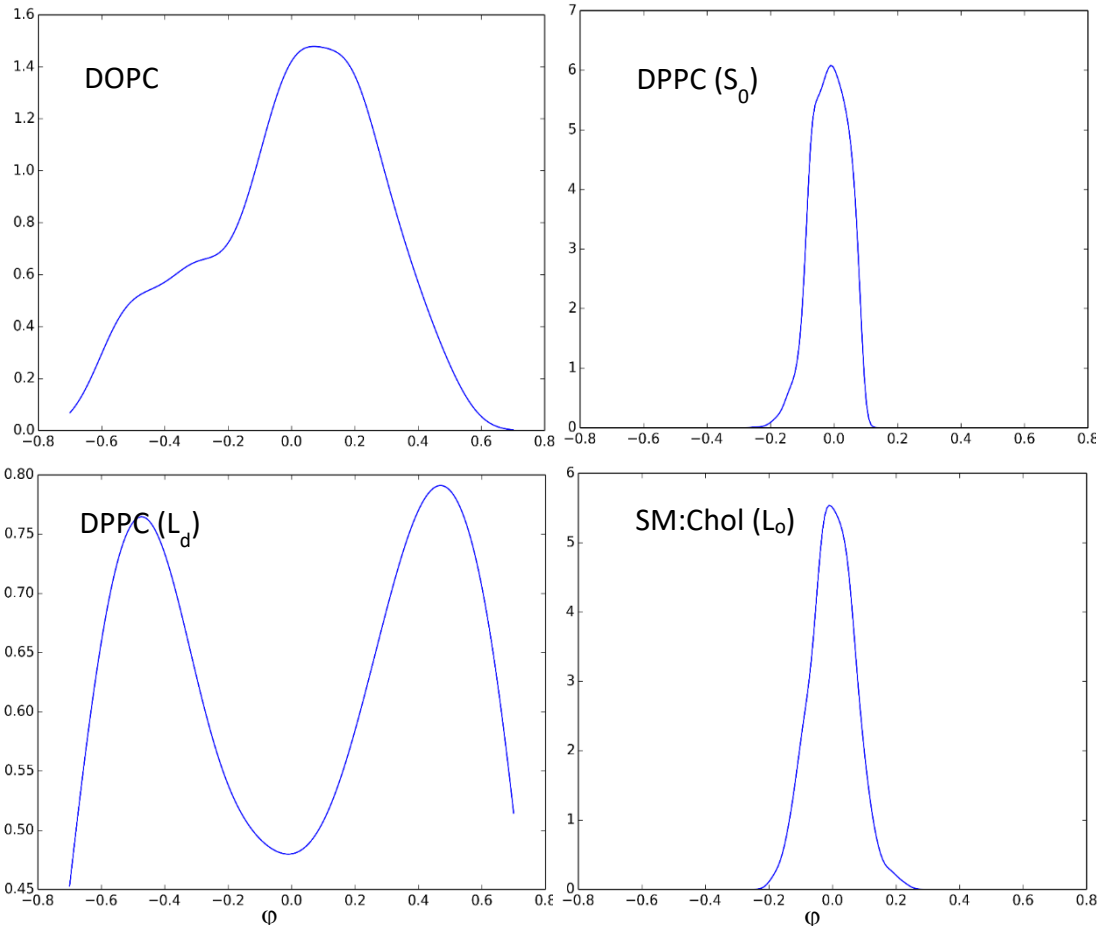

Figure S8: Density plots for the vector of the transition dipole moment in function of the azimuthal angle φ for the four membranes. It denotes the angle in the plane of the membrane in radians. Since the x-axis in the plane of the membrane (to which is referred by the φ-angle) is not uniquely defined, in these plots 0 radians is taken as the midpoint of the sampled angles. For DOPC, the two symmetric peaks are covered within the maximum at φ=0.0 and 0.2 radians.

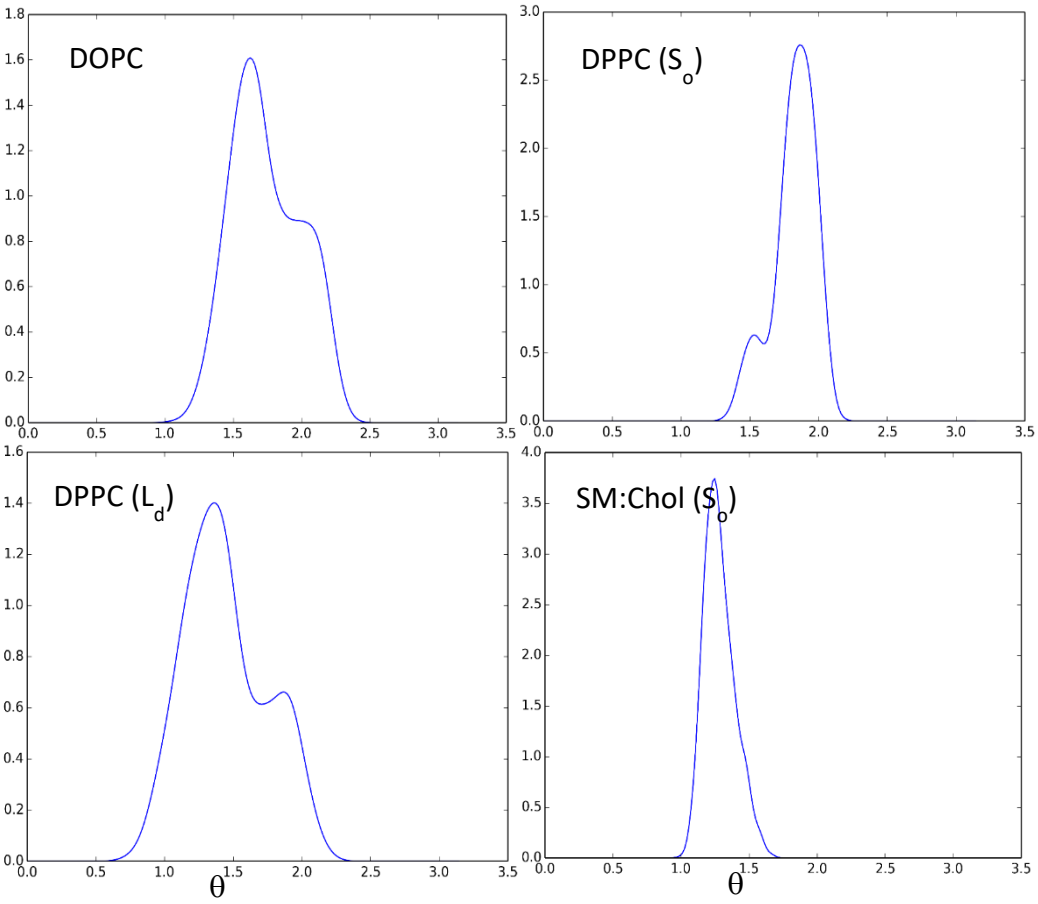

Figure S9: Density plots for the vector of the transition dipole moment in function of the angle θ for the four membranes. It denotes the angle between the transition dipole moment and the z-axis of the membrane in radians. The first peak for DPPC (S_o) (at θ= 1.4 rad) and the second peak for DPPC (L_d) (at θ=1.9 rad) are less expressed due to a limited simulation time.

Table S1: dii.itp

```
; Charges were computed with RED and Duan method: b3lyp/cc-pVTZ
SCRF(IEFPCM,Solvent=diethylether)
;       This file was generated by PRODRG version AA100323.0717
;       PRODRG written/copyrighted by Daan van Aalten
;       and Alexander Schuettelkopf
;
;       Questions/comments to dava@davapc1.bioch.dundee.ac.uk
;
;       When using this software in a publication, cite:
;       A. W. Schuettelkopf and D. M. F. van Aalten (2004).
;       PRODRG - a tool for high-throughput crystallography
;       of protein-ligand complexes.
;       Acta Crystallogr. D60, 1355--1363.
;
;

[ moleculetype ]
; Name nrexcl
LIG      3

[ atoms ]
     1       CH3     1  LIG     CBS     1  -0.0285  15.0350
     2       CH2     1  LIG     CBR     1   0.0271  14.0270
     3       CH2     1  LIG     CBQ     1   0.0076  14.0270
     4       CH2     1  LIG     CBP     1   -0.0071  14.0270
     5       CH2     1  LIG     CBO     1   -0.0019  14.0270
     6       CH2     1  LIG     CBN     1   0.0056  14.0270
     7       CH2     1  LIG     CBM     1   -0.0004  14.0270
     8       CH2     1  LIG     CBL     2   -0.0012  14.0270
     9       CH2     1  LIG     CBK     2   0.0004  14.0270
    10       CH2     1  LIG     CBJ     2   0.0035  14.0270
    11       CH2     1  LIG     CBI     2   -0.0004  14.0270
    12       CH2     1  LIG     CBH     3   -0.0011  14.0270
    13       CH2     1  LIG     CBG     3   0.0071  14.0270
    14       CH2     1  LIG     CBF     3   0.0109  14.0270
    15       CH2     1  LIG     CBE     3   0.0007  14.0270
    16       CH2     1  LIG     CBD     3  0.0068  14.0270
    17       CH2     1  LIG     CBC     4   0.0932  14.0270
    18       CH2     1  LIG     CBB     4  0.1068  14.0270
    19        NR     1  LIG     NBA     4   0.0572  14.0067
    20         C     1  LIG     CAT     4   0.0180  12.0110
    21       CR1     1  LIG     CAV     4  -0.1198  12.0110
    22        HC     1  LIG     HAV     4   0.1042   1.0080
    23       CR1     1  LIG     CAX     4  -0.1396  12.0110
    24        HC     1  LIG     HAX     4   0.1405   1.0080
    25       CR1     1  LIG     CAW     4  -0.1166  12.0110
    26        HC     1  LIG     HAW     4   0.1311   1.0080
    27       CR1     1  LIG     CAU     5  -0.1906  12.0110
    28        HC     1  LIG     HAU     5   0.1593   1.0080
    29         C     1  LIG     CAS     5   0.0317  12.0110
    30       CH2     1  LIG     CAR     5   0.1061  12.0110
    31       CH3     1  LIG     CAY     5  0.0298  15.0350
    32       CH3     1  LIG     CAZ     5  0.0276  15.0350
    33         C     1  LIG     CAQ     6   0.0321  12.0110
    34         C     1  LIG     CAP     6  -0.0785  13.0190
    35         C     1  LIG     CAO     6  0.0792  13.0190
    36         C     1  LIG     CAN     7  -0.0032  13.0190
    37         C     1  LIG     CAM     7  0.0792  13.0190
    38         C     1  LIG     CAL     7  -0.0711  13.0190
    39         C     1  LIG     CAH     7   0.0323  12.0110
    40       CH2     1  LIG     CAG     7   0.0942  12.0110
    41       CH3     1  LIG     CAJ     7  0.0284  15.0350
    42       CH3     1  LIG     CAK     7  0.0316  15.0350
    43         C     1  LIG     CAD     8   0.0394  12.0110
```

```
    44       CR1     1  LIG     CAE     8  -0.1866  12.0110
    45        HC     1  LIG     HAE     8   0.1566   1.0080
    46       CR1     1  LIG     CAF     8  -0.1278  12.0110
    47        HC     1  LIG     HAF     8   0.1335   1.0080
    48       CR1     1  LIG     CAA     8  -0.1302  12.0110
    49        HC     1  LIG     HAA     8   0.1381   1.0080
    50       CR1     1  LIG     CAB     8  -0.1192  12.0110
    51        HC     1  LIG     HAB     8   0.1018   1.0080
    52         C     1  LIG     CAC     8   0.0206  12.0110
    53        NR     1  LIG     NAI     8   0.0540  14.0067
    54       CH2     1  LIG     CBT     9  0.1048  14.0270
    55       CH2     1  LIG     CBU     9   0.0926  14.0270
    56       CH2     1  LIG     CBV     9  0.0074  14.0270
    57       CH2     1  LIG     CBW     9   0.0013  14.0270
    58       CH2     1  LIG     CBX     9   0.0101  14.0270
    59       CH2     1  LIG     CBY    10   0.008  14.0270
    60       CH2     1  LIG     CBZ    10   -0.0018  14.0270
    61       CH2     1  LIG     CCA    10   0.0006  14.0270
    62       CH2     1  LIG     CCB    10   0.0026  14.0270
    63       CH2     1  LIG     CCC    10   0.0013  14.0270
    64       CH2     1  LIG     CCD    10   -0.0018  14.0270
    65       CH2     1  LIG     CCE    11   0.0002  14.0270
    66       CH2     1  LIG     CCF    11   0.0048  14.0270
    67       CH2     1  LIG     CCG    11   -0.0006  14.0270
    68       CH2     1  LIG     CCH    11   -0.0088  14.0270
    69       CH2     1  LIG     CCI    11   0.0079  14.0270
    70       CH2     1  LIG     CCJ    11   0.0259  14.0270
    71       CH3     1  LIG     CCK    11  -0.0269  15.0350

[ bonds ]
; ai  aj  fu    c0, c1, ...
   2   1   2    0.153   7150000.0    0.153   7150000.0 ;   CBR  CBS
   2   3   2    0.153   7150000.0    0.153   7150000.0 ;   CBR  CBQ
   3   4   2    0.153   7150000.0    0.153   7150000.0 ;   CBQ  CBP
   4   5   2    0.153   7150000.0    0.153   7150000.0 ;   CBP  CBO
   5   6   2    0.153   7150000.0    0.153   7150000.0 ;   CBO  CBN
   6   7   2    0.153   7150000.0    0.153   7150000.0 ;   CBN  CBM
   7   8   2    0.153   7150000.0    0.153   7150000.0 ;   CBM  CBL
   8   9   2    0.153   7150000.0    0.153   7150000.0 ;   CBL  CBK
   9  10   2    0.153   7150000.0    0.153   7150000.0 ;   CBK  CBJ
  10  11   2    0.153   7150000.0    0.153   7150000.0 ;   CBJ  CBI
  11  12   2    0.153   7150000.0    0.153   7150000.0 ;   CBI  CBH
  12  13   2    0.153   7150000.0    0.153   7150000.0 ;   CBH  CBG
  13  14   2    0.153   7150000.0    0.153   7150000.0 ;   CBG  CBF
  14  15   2    0.153   7150000.0    0.153   7150000.0 ;   CBF  CBE
  15  16   2    0.153   7150000.0    0.153   7150000.0 ;   CBE  CBD
  16  17   2    0.153   7150000.0    0.153   7150000.0 ;   CBD  CBC
  17  18   2    0.153   7150000.0    0.153   7150000.0 ;   CBC  CBB
  19  18   2    0.148   5730000.0    0.148   5730000.0 ;   NBA  CBB
  19  20   2    0.133  11800000.0    0.133  11800000.0 ;   NBA  CAT
  19  33   2    0.133  11800000.0    0.133  11800000.0 ;   NBA  CAQ
  20  21   2    0.133  11800000.0    0.133  11800000.0 ;   CAT  CAV
  20  29   2    0.133  11800000.0    0.133  11800000.0 ;   CAT  CAS
  21  22   2    0.109  12300000.0    0.109  12300000.0 ;   CAV  HAV
  21  23   2    0.139  10800000.0    0.139  10800000.0 ;   CAV  CAX
  23  24   2    0.109  12300000.0    0.109  12300000.0 ;   CAX  HAX
  23  25   2    0.139  10800000.0    0.139  10800000.0 ;   CAX  CAW
  25  26   2    0.109  12300000.0    0.109  12300000.0 ;   CAW  HAW
  25  27   2    0.139  10800000.0    0.139  10800000.0 ;   CAW  CAU
  27  28   2    0.109  12300000.0    0.109  12300000.0 ;   CAU  HAU
  29  27   2    0.133  11800000.0    0.133  11800000.0 ;   CAS  CAU
  30  29   2    0.139   8660000.0    0.139   8660000.0 ;   CAR  CAS
  30  31   2    0.153   7150000.0    0.153   7150000.0 ;   CAR  CAY
  30  32   2    0.153   7150000.0    0.153   7150000.0 ;   CAR  CAZ
  30  33   2    0.139   8660000.0    0.139   8660000.0 ;   CAR  CAQ
  33  34   2    0.133  11800000.0    0.133  11800000.0 ;   CAQ  CAP
  34  35   2    0.153   7150000.0    0.153   7150000.0 ;   CAP  CAO
  35  36   2    0.153   7150000.0    0.153   7150000.0 ;   CAO  CAN
  36  37   2    0.153   7150000.0    0.153   7150000.0 ;   CAN  CAM
```

```
  37  38   2    0.153   7150000.0    0.153   7150000.0 ;   CAM  CAL
  39  38   2    0.133  11800000.0    0.133  11800000.0 ;   CAH  CAL
  40  39   2    0.139   8660000.0    0.139   8660000.0 ;   CAG  CAH
  39  53   2    0.133  11800000.0    0.133  11800000.0 ;   CAH  NAI
  40  41   2    0.153   7150000.0    0.153   7150000.0 ;   CAG  CAJ
  40  42   2    0.153   7150000.0    0.153   7150000.0 ;   CAG  CAK
  40  43   2    0.139   8660000.0    0.139   8660000.0 ;   CAG  CAD
  43  44   2    0.133  11800000.0    0.133  11800000.0 ;   CAD  CAE
  43  52   2    0.133  11800000.0    0.133  11800000.0 ;   CAD  CAC
  44  45   2    0.109  12300000.0    0.109  12300000.0 ;   CAE  HAE
  44  46   2    0.139  10800000.0    0.139  10800000.0 ;   CAE  CAF
  46  47   2    0.109  12300000.0    0.109  12300000.0 ;   CAF  HAF
  46  48   2    0.139  10800000.0    0.139  10800000.0 ;   CAF  CAA
  48  49   2    0.109  12300000.0    0.109  12300000.0 ;   CAA  HAA
  48  50   2    0.139  10800000.0    0.139  10800000.0 ;   CAA  CAB
  50  51   2    0.109  12300000.0    0.109  12300000.0 ;   CAB  HAB
  52  50   2    0.133  11800000.0    0.133  11800000.0 ;   CAC  CAB
  52  53   2    0.133  11800000.0    0.133  11800000.0 ;   CAC  NAI
  53  54   2    0.148   5730000.0    0.148   5730000.0 ;   NAI  CBT
  54  55   2    0.153   7150000.0    0.153   7150000.0 ;   CBT  CBU
  55  56   2    0.153   7150000.0    0.153   7150000.0 ;   CBU  CBV
  56  57   2    0.153   7150000.0    0.153   7150000.0 ;   CBV  CBW
  57  58   2    0.153   7150000.0    0.153   7150000.0 ;   CBW  CBX
  58  59   2    0.153   7150000.0    0.153   7150000.0 ;   CBX  CBY
  59  60   2    0.153   7150000.0    0.153   7150000.0 ;   CBY  CBZ
  60  61   2    0.153   7150000.0    0.153   7150000.0 ;   CBZ  CCA
  61  62   2    0.153   7150000.0    0.153   7150000.0 ;   CCA  CCB
  62  63   2    0.153   7150000.0    0.153   7150000.0 ;   CCB  CCC
  63  64   2    0.153   7150000.0    0.153   7150000.0 ;   CCC  CCD
  64  65   2    0.153   7150000.0    0.153   7150000.0 ;   CCD  CCE
  65  66   2    0.153   7150000.0    0.153   7150000.0 ;   CCE  CCF
  66  67   2    0.153   7150000.0    0.153   7150000.0 ;   CCF  CCG
  67  68   2    0.153   7150000.0    0.153   7150000.0 ;   CCG  CCH
  68  69   2    0.153   7150000.0    0.153   7150000.0 ;   CCH  CCI
  69  70   2    0.153   7150000.0    0.153   7150000.0 ;   CCI  CCJ
  70  71   2    0.153   7150000.0    0.153   7150000.0 ;   CCJ  CCK

[ pairs ]
; ai  aj  fu    c0, c1, ...
   1   4   1                                            ;   CBS  CBP
   2   5   1                                            ;   CBR  CBO
   3   6   1                                            ;   CBQ  CBN
   4   7   1                                            ;   CBP  CBM
   5   8   1                                            ;   CBO  CBL
   6   9   1                                            ;   CBN  CBK
   7  10   1                                            ;   CBM  CBJ
   8  11   1                                            ;   CBL  CBI
   9  12   1                                            ;   CBK  CBH
  10  13   1                                            ;   CBJ  CBG
  11  14   1                                            ;   CBI  CBF
  12  15   1                                            ;   CBH  CBE
  13  16   1                                            ;   CBG  CBD
  14  17   1                                            ;   CBF  CBC
  15  18   1                                            ;   CBE  CBB
  16  19   1                                            ;   CBD  NBA
  17  20   1                                            ;   CBC  CAT
  17  33   1                                            ;   CBC  CAQ
  18  21   1                                            ;   CBB  CAV
  18  29   1                                            ;   CBB  CAS
  18  30   1                                            ;   CBB  CAR
  18  34   1                                            ;   CBB  CAP
  19  22   1                                            ;   NBA  HAV
  19  23   1                                            ;   NBA  CAX
  19  27   1                                            ;   NBA  CAU
  19  31   1                                            ;   NBA  CAY
  19  32   1                                            ;   NBA  CAZ
  19  35   1                                            ;   NBA  CAO
  20  24   1                                            ;   CAT  HAX
  20  25   1                                            ;   CAT  CAW
```

```
20  28   1                                   ;   CAT  HAU
20  31   1                                   ;   CAT  CAY
20  32   1                                   ;   CAT  CAZ
20  34   1                                   ;   CAT  CAP
21  26   1                                   ;   CAV  HAW
21  27   1                                   ;   CAV  CAU
21  30   1                                   ;   CAV  CAR
21  33   1                                   ;   CAV  CAQ
22  24   1                                   ;   HAV  HAX
22  25   1                                   ;   HAV  CAW
22  29   1                                   ;   HAV  CAS
23  28   1                                   ;   CAX  HAU
23  29   1                                   ;   CAX  CAS
24  26   1                                   ;   HAX  HAW
24  27   1                                   ;   HAX  CAU
25  30   1                                   ;   CAW  CAR
26  28   1                                   ;   HAW  HAU
26  29   1                                   ;   HAW  CAS
27  31   1                                   ;   CAU  CAY
27  32   1                                   ;   CAU  CAZ
27  33   1                                   ;   CAU  CAQ
28  30   1                                   ;   HAU  CAR
29  34   1                                   ;   CAS  CAP
30  35   1                                   ;   CAR  CAO
31  34   1                                   ;   CAY  CAP
32  34   1                                   ;   CAZ  CAP
33  36   1                                   ;   CAQ  CAN
34  37   1                                   ;   CAP  CAM
35  38   1                                   ;   CAO  CAL
36  39   1                                   ;   CAN  CAH
37  40   1                                   ;   CAM  CAG
37  53   1                                   ;   CAM  NAI
38  41   1                                   ;   CAL  CAJ
38  42   1                                   ;   CAL  CAK
38  43   1                                   ;   CAL  CAD
38  52   1                                   ;   CAL  CAC
38  54   1                                   ;   CAL  CBT
39  44   1                                   ;   CAH  CAE
39  50   1                                   ;   CAH  CAB
39  55   1                                   ;   CAH  CBU
40  45   1                                   ;   CAG  HAE
40  46   1                                   ;   CAG  CAF
40  50   1                                   ;   CAG  CAB
40  54   1                                   ;   CAG  CBT
41  44   1                                   ;   CAJ  CAE
41  52   1                                   ;   CAJ  CAC
41  53   1                                   ;   CAJ  NAI
42  44   1                                   ;   CAK  CAE
42  52   1                                   ;   CAK  CAC
42  53   1                                   ;   CAK  NAI
43  47   1                                   ;   CAD  HAF
43  48   1                                   ;   CAD  CAA
43  51   1                                   ;   CAD  HAB
43  54   1                                   ;   CAD  CBT
44  49   1                                   ;   CAE  HAA
44  50   1                                   ;   CAE  CAB
44  53   1                                   ;   CAE  NAI
45  47   1                                   ;   HAE  HAF
45  48   1                                   ;   HAE  CAA
45  52   1                                   ;   HAE  CAC
46  51   1                                   ;   CAF  HAB
46  52   1                                   ;   CAF  CAC
47  49   1                                   ;   HAF  HAA
47  50   1                                   ;   HAF  CAB
48  53   1                                   ;   CAA  NAI
49  51   1                                   ;   HAA  HAB
49  52   1                                   ;   HAA  CAC
50  54   1                                   ;   CAB  CBT
51  53   1                                   ;   HAB  NAI
```

```
  52  55   1                                          ;   CAC  CBU
  53  56   1                                          ;   NAI  CBV
  54  57   1                                          ;   CBT  CBW
  55  58   1                                          ;   CBU  CBX
  56  59   1                                          ;   CBV  CBY
  57  60   1                                          ;   CBW  CBZ
  58  61   1                                          ;   CBX  CCA
  59  62   1                                          ;   CBY  CCB
  60  63   1                                          ;   CBZ  CCC
  61  64   1                                          ;   CCA  CCD
  62  65   1                                          ;   CCB  CCE
  63  66   1                                          ;   CCC  CCF
  64  67   1                                          ;   CCD  CCG
  65  68   1                                          ;   CCE  CCH
  66  69   1                                          ;   CCF  CCI
  67  70   1                                          ;   CCG  CCJ
  68  71   1                                          ;   CCH  CCK

[ angles ]
; ai  aj  ak  fu    c0, c1, ...
   1   2   3   2    109.5       520.0    109.5       520.0 ;   CBS  CBR  CBQ
   2   3   4   2    109.5       520.0    109.5       520.0 ;   CBR  CBQ  CBP
   3   4   5   2    109.5       520.0    109.5       520.0 ;   CBQ  CBP  CBO
   4   5   6   2    109.5       520.0    109.5       520.0 ;   CBP  CBO  CBN
   5   6   7   2    109.5       520.0    109.5       520.0 ;   CBO  CBN  CBM
   6   7   8   2    109.5       520.0    109.5       520.0 ;   CBN  CBM  CBL
   7   8   9   2    109.5       520.0    109.5       520.0 ;   CBM  CBL  CBK
   8   9  10   2    109.5       520.0    109.5       520.0 ;   CBL  CBK  CBJ
   9  10  11   2    109.5       520.0    109.5       520.0 ;   CBK  CBJ  CBI
  10  11  12   2    109.5       520.0    109.5       520.0 ;   CBJ  CBI  CBH
  11  12  13   2    109.5       520.0    109.5       520.0 ;   CBI  CBH  CBG
  12  13  14   2    109.5       520.0    109.5       520.0 ;   CBH  CBG  CBF
  13  14  15   2    109.5       520.0    109.5       520.0 ;   CBG  CBF  CBE
  14  15  16   2    109.5       520.0    109.5       520.0 ;   CBF  CBE  CBD
  15  16  17   2    109.5       520.0    109.5       520.0 ;   CBE  CBD  CBC
  16  17  18   2    109.5       520.0    109.5       520.0 ;   CBD  CBC  CBB
  17  18  19   2    111.0       530.0    111.0       530.0 ;   CBC  CBB  NBA
  18  19  20   2    125.0       375.0    125.0       375.0 ;   CBB  NBA  CAT
  18  19  33   2    125.0       375.0    125.0       375.0 ;   CBB  NBA  CAQ
  20  19  33   2    108.0       465.0    108.0       465.0 ;   CAT  NBA  CAQ
  19  20  21   2    132.0       760.0    132.0       760.0 ;   NBA  CAT  CAV
  19  20  29   2    108.0       465.0    108.0       465.0 ;   NBA  CAT  CAS
  21  20  29   2    120.0       560.0    120.0       560.0 ;   CAV  CAT  CAS
  20  21  22   2    120.0       505.0    120.0       505.0 ;   CAT  CAV  HAV
  20  21  23   2    120.0       505.0    120.0       505.0 ;   CAT  CAV  CAX
  22  21  23   2    120.0       505.0    120.0       505.0 ;   HAV  CAV  CAX
  21  23  24   2    120.0       505.0    120.0       505.0 ;   CAV  CAX  HAX
  21  23  25   2    120.0       505.0    120.0       505.0 ;   CAV  CAX  CAW
  24  23  25   2    120.0       505.0    120.0       505.0 ;   HAX  CAX  CAW
  23  25  26   2    120.0       505.0    120.0       505.0 ;   CAX  CAW  HAW
  23  25  27   2    120.0       505.0    120.0       505.0 ;   CAX  CAW  CAU
  26  25  27   2    120.0       505.0    120.0       505.0 ;   HAW  CAW  CAU
  25  27  28   2    120.0       505.0    120.0       505.0 ;   CAW  CAU  HAU
  25  27  29   2    120.0       505.0    120.0       505.0 ;   CAW  CAU  CAS
  28  27  29   2    120.0       505.0    120.0       505.0 ;   HAU  CAU  CAS
  20  29  27   2    120.0       560.0    120.0       560.0 ;   CAT  CAS  CAU
  20  29  30   2    108.0       465.0    108.0       465.0 ;   CAT  CAS  CAR
  27  29  30   2    132.0       760.0    132.0       760.0 ;   CAU  CAS  CAR
  29  30  31   2    109.5       520.0    109.5       520.0 ;   CAS  CAR  CAY
  29  30  32   2    109.5       520.0    109.5       520.0 ;   CAS  CAR  CAZ
  29  30  33   2    104.0       444.4    104.0       444.4 ;   CAS  CAR  CAQ
  31  30  32   2    109.5       520.0    109.5       520.0 ;   CAY  CAR  CAZ
  31  30  33   2    109.5       520.0    109.5       520.0 ;   CAY  CAR  CAQ
  32  30  33   2    109.5       520.0    109.5       520.0 ;   CAZ  CAR  CAQ
  19  33  30   2    108.0       465.0    108.0       465.0 ;   NBA  CAQ  CAR
  19  33  34   2    120.0       560.0    120.0       560.0 ;   NBA  CAQ  CAP
  30  33  34   2    120.0       560.0    120.0       560.0 ;   CAR  CAQ  CAP
  33  34  35   2    115.0       610.0    115.0       610.0 ;   CAQ  CAP  CAO
  34  35  36   2    115.0       610.0    115.0       610.0 ;   CAP  CAO  CAN
```

```
  35  36  37   2    115.0       610.0    115.0       610.0 ;   CAO  CAN  CAM
  36  37  38   2    115.0       610.0    115.0       610.0 ;   CAN  CAM  CAL
  37  38  39   2    115.0       610.0    115.0       610.0 ;   CAM  CAL  CAH
  38  39  40   2    120.0       560.0    120.0       560.0 ;   CAL  CAH  CAG
  38  39  53   2    120.0       560.0    120.0       560.0 ;   CAL  CAH  NAI
  40  39  53   2    108.0       465.0    108.0       465.0 ;   CAG  CAH  NAI
  39  40  41   2    109.5       520.0    109.5       520.0 ;   CAH  CAG  CAJ
  39  40  42   2    109.5       520.0    109.5       520.0 ;   CAH  CAG  CAK
  39  40  43   2    104.0       444.4    104.0       444.4 ;   CAH  CAG  CAD
  41  40  42   2    109.5       520.0    109.5       520.0 ;   CAJ  CAG  CAK
  41  40  43   2    109.5       520.0    109.5       520.0 ;   CAJ  CAG  CAD
  42  40  43   2    109.5       520.0    109.5       520.0 ;   CAK  CAG  CAD
  40  43  44   2    132.0       760.0    132.0       760.0 ;   CAG  CAD  CAE
  40  43  52   2    108.0       465.0    108.0       465.0 ;   CAG  CAD  CAC
  44  43  52   2    120.0       560.0    120.0       560.0 ;   CAE  CAD  CAC
  43  44  45   2    120.0       505.0    120.0       505.0 ;   CAD  CAE  HAE
  43  44  46   2    120.0       505.0    120.0       505.0 ;   CAD  CAE  CAF
  45  44  46   2    120.0       505.0    120.0       505.0 ;   HAE  CAE  CAF
  44  46  47   2    120.0       505.0    120.0       505.0 ;   CAE  CAF  HAF
  44  46  48   2    120.0       505.0    120.0       505.0 ;   CAE  CAF  CAA
  47  46  48   2    120.0       505.0    120.0       505.0 ;   HAF  CAF  CAA
  46  48  49   2    120.0       505.0    120.0       505.0 ;   CAF  CAA  HAA
  46  48  50   2    120.0       505.0    120.0       505.0 ;   CAF  CAA  CAB
  49  48  50   2    120.0       505.0    120.0       505.0 ;   HAA  CAA  CAB
  48  50  51   2    120.0       505.0    120.0       505.0 ;   CAA  CAB  HAB
  48  50  52   2    120.0       505.0    120.0       505.0 ;   CAA  CAB  CAC
  51  50  52   2    120.0       505.0    120.0       505.0 ;   HAB  CAB  CAC
  43  52  50   2    120.0       560.0    120.0       560.0 ;   CAD  CAC  CAB
  43  52  53   2    108.0       465.0    108.0       465.0 ;   CAD  CAC  NAI
  50  52  53   2    132.0       760.0    132.0       760.0 ;   CAB  CAC  NAI
  39  53  52   2    108.0       465.0    108.0       465.0 ;   CAH  NAI  CAC
  39  53  54   2    125.0       375.0    125.0       375.0 ;   CAH  NAI  CBT
  52  53  54   2    125.0       375.0    125.0       375.0 ;   CAC  NAI  CBT
  53  54  55   2    111.0       530.0    111.0       530.0 ;   NAI  CBT  CBU
  54  55  56   2    109.5       520.0    109.5       520.0 ;   CBT  CBU  CBV
  55  56  57   2    109.5       520.0    109.5       520.0 ;   CBU  CBV  CBW
  56  57  58   2    109.5       520.0    109.5       520.0 ;   CBV  CBW  CBX
  57  58  59   2    109.5       520.0    109.5       520.0 ;   CBW  CBX  CBY
  58  59  60   2    109.5       520.0    109.5       520.0 ;   CBX  CBY  CBZ
  59  60  61   2    109.5       520.0    109.5       520.0 ;   CBY  CBZ  CCA
  60  61  62   2    109.5       520.0    109.5       520.0 ;   CBZ  CCA  CCB
  61  62  63   2    109.5       520.0    109.5       520.0 ;   CCA  CCB  CCC
  62  63  64   2    109.5       520.0    109.5       520.0 ;   CCB  CCC  CCD
  63  64  65   2    109.5       520.0    109.5       520.0 ;   CCC  CCD  CCE
  64  65  66   2    109.5       520.0    109.5       520.0 ;   CCD  CCE  CCF
  65  66  67   2    109.5       520.0    109.5       520.0 ;   CCE  CCF  CCG
  66  67  68   2    109.5       520.0    109.5       520.0 ;   CCF  CCG  CCH
  67  68  69   2    109.5       520.0    109.5       520.0 ;   CCG  CCH  CCI
  68  69  70   2    109.5       520.0    109.5       520.0 ;   CCH  CCI  CCJ
  69  70  71   2    109.5       520.0    109.5       520.0 ;   CCI  CCJ  CCK

[ dihedrals ]
; ai  aj  ak  al  fu    c0, c1, m, ...
  19  18  33  20   2      0.0  167.4        0.0  167.4   ; imp   NBA  CBB  CAQ  CAT
  20  19  21  29   2      0.0  167.4        0.0  167.4   ; imp   CAT  NBA  CAV  CAS
  21  20  23  22   2      0.0  167.4        0.0  167.4   ; imp   CAV  CAT  CAX  HAV
  23  21  25  24   2      0.0  167.4        0.0  167.4   ; imp   CAX  CAV  CAW  HAX
  25  23  27  26   2      0.0  167.4        0.0  167.4   ; imp   CAW  CAX  CAU  HAW
  27  25  29  28   2      0.0  167.4        0.0  167.4   ; imp   CAU  CAW  CAS  HAU
  29  30  27  20   2      0.0  167.4        0.0  167.4   ; imp   CAS  CAR  CAU  CAT
  30  29  32  31   2     35.3  334.8       35.3  334.8   ; imp   CAR  CAS  CAZ  CAY
  33  34  30  19   2      0.0  167.4        0.0  167.4   ; imp   CAQ  CAP  CAR  NBA
  39  38  40  53   2      0.0  167.4        0.0  167.4   ; imp   CAH  CAL  CAG  NAI
  40  39  42  41   2     35.3  334.8       35.3  334.8   ; imp   CAG  CAH  CAK  CAJ
  43  40  44  52   2      0.0  167.4        0.0  167.4   ; imp   CAD  CAG  CAE  CAC
  44  43  46  45   2      0.0  167.4        0.0  167.4   ; imp   CAE  CAD  CAF  HAE
  46  44  48  47   2      0.0  167.4        0.0  167.4   ; imp   CAF  CAE  CAA  HAF
  48  46  50  49   2      0.0  167.4        0.0  167.4   ; imp   CAA  CAF  CAB  HAA
  50  48  52  51   2      0.0  167.4        0.0  167.4   ; imp   CAB  CAA  CAC  HAB
```

```
  52  53  50  43   2      0.0  167.4        0.0  167.4   ; imp   CAC  NAI  CAB  CAD
  53  54  52  39   2      0.0  167.4        0.0  167.4   ; imp   NAI  CBT  CAC  CAH
  43  44  46  48   2      0.0  209.3        0.0  209.3   ; imp   CAD  CAE  CAF  CAA
  44  46  48  50   2      0.0  209.3        0.0  209.3   ; imp   CAE  CAF  CAA  CAB
  46  48  50  52   2      0.0  209.3        0.0  209.3   ; imp   CAF  CAA  CAB  CAC
  48  50  52  43   2      0.0  209.3        0.0  209.3   ; imp   CAA  CAB  CAC  CAD
  50  52  43  44   2      0.0  209.3        0.0  209.3   ; imp   CAB  CAC  CAD  CAE
  52  43  44  46   2      0.0  209.3        0.0  209.3   ; imp   CAC  CAD  CAE  CAF
  20  21  23  25   2      0.0  209.3        0.0  209.3   ; imp   CAT  CAV  CAX  CAW
  21  23  25  27   2      0.0  209.3        0.0  209.3   ; imp   CAV  CAX  CAW  CAU
  23  25  27  29   2      0.0  209.3        0.0  209.3   ; imp   CAX  CAW  CAU  CAS
  25  27  29  20   2      0.0  209.3        0.0  209.3   ; imp   CAW  CAU  CAS  CAT
  27  29  20  21   2      0.0  209.3        0.0  209.3   ; imp   CAU  CAS  CAT  CAV
  29  20  21  23   2      0.0  209.3        0.0  209.3   ; imp   CAS  CAT  CAV  CAX
   4   3   2   1   1      0.0    5.9 3      0.0    5.9 3 ; dih   CBP  CBQ  CBR  CBS
   5   4   3   2   1      0.0    5.9 3      0.0    5.9 3 ; dih   CBO  CBP  CBQ  CBR
   6   5   4   3   1      0.0    5.9 3      0.0    5.9 3 ; dih   CBN  CBO  CBP  CBQ
   7   6   5   4   1      0.0    5.9 3      0.0    5.9 3 ; dih   CBM  CBN  CBO  CBP
   8   7   6   5   1      0.0    5.9 3      0.0    5.9 3 ; dih   CBL  CBM  CBN  CBO
   9   8   7   6   1      0.0    5.9 3      0.0    5.9 3 ; dih   CBK  CBL  CBM  CBN
  10   9   8   7   1      0.0    5.9 3      0.0    5.9 3 ; dih   CBJ  CBK  CBL  CBM
  11  10   9   8   1      0.0    5.9 3      0.0    5.9 3 ; dih   CBI  CBJ  CBK  CBL
  12  11  10   9   1      0.0    5.9 3      0.0    5.9 3 ; dih   CBH  CBI  CBJ  CBK
  13  12  11  10   1      0.0    5.9 3      0.0    5.9 3 ; dih   CBG  CBH  CBI  CBJ
  14  13  12  11   1      0.0    5.9 3      0.0    5.9 3 ; dih   CBF  CBG  CBH  CBI
  15  14  13  12   1      0.0    5.9 3      0.0    5.9 3 ; dih   CBE  CBF  CBG  CBH
  16  15  14  13   1      0.0    5.9 3      0.0    5.9 3 ; dih   CBD  CBE  CBF  CBG
  17  16  15  14   1      0.0    5.9 3      0.0    5.9 3 ; dih   CBC  CBD  CBE  CBF
  18  17  16  15   1      0.0    5.9 3      0.0    5.9 3 ; dih   CBB  CBC  CBD  CBE
  19  18  17  16   1      0.0    5.9 3      0.0    5.9 3 ; dih   NBA  CBB  CBC  CBD
  17  18  19  33   1      0.0    1.0 6      0.0    1.0 6 ; dih   CBC  CBB  NBA  CAQ
  29  20  19  18   1    180.0   33.5 2    180.0   33.5 2 ; dih   CAS  CAT  NBA  CBB
  34  33  19  18   1    180.0   33.5 2    180.0   33.5 2 ; dih   CAP  CAQ  NBA  CBB
  33  30  29  20   1    180.0   33.5 2    180.0   33.5 2 ; dih   CAQ  CAR  CAS  CAT
set as double bond
  29  30  33  34   1    180.0   33.5 2    180.0   33.5 2 ; dih   CAS  CAR  CAQ  CAP
set as double bond
  35  34  33  19   1    180.0   16.7 2    180.0   16.7 2 ; dih   CAO  CAP  CAQ  NBA
gd_12 from RTOL
  36  35  34  33   1    180.0   33.5 2    180.0   33.5 2 ; dih   CAN  CAO  CAP  CAQ
gd_14 from RTOL
  37  36  35  34   1    180.0   16.7 2    180.0   16.7 2 ; dih   CAM  CAN  CAO  CAP
gd_12 from RTOL
  38  37  36  35   1    180.0   33.5 2    180.0   33.5 2 ; dih   CAL  CAM  CAN  CAO
gd_14 from RTOL
  39  38  37  36   1    180.0   16.7 2    180.0   16.7 2 ; dih   CAH  CAL  CAM  CAN
gd_12 from RTOL
  53  39  38  37   1    180.0   33.5 2    180.0   33.5 2 ; dih   NAI  CAH  CAL  CAM
gd_14 from RTOL
  43  40  39  38   1    180.0   33.5 2    180.0   33.5 2 ; dih   CAD  CAG  CAH  CAL
set as double bond
  38  39  53  54   1    180.0   33.5 2    180.0   33.5 2 ; dih   CAL  CAH  NAI  CBT
set as double bond
  39  40  43  52   1    180.0   33.5 2    180.0   33.5 2 ; dih   CAH  CAG  CAD  CAC
  43  52  53  54   1    180.0   33.5 2    180.0   33.5 2 ; dih   CAD  CAC  NAI  CBT
  55  54  53  39   1      0.0    1.0 6      0.0    1.0 6 ; dih   CBU  CBT  NAI  CAH
  56  55  54  53   1      0.0    5.9 3      0.0    5.9 3 ; dih   CBV  CBU  CBT  NAI
  57  56  55  54   1      0.0    5.9 3      0.0    5.9 3 ; dih   CBW  CBV  CBU  CBT
  58  57  56  55   1      0.0    5.9 3      0.0    5.9 3 ; dih   CBX  CBW  CBV  CBU
  59  58  57  56   1      0.0    5.9 3      0.0    5.9 3 ; dih   CBY  CBX  CBW  CBV
  60  59  58  57   1      0.0    5.9 3      0.0    5.9 3 ; dih   CBZ  CBY  CBX  CBW
  61  60  59  58   1      0.0    5.9 3      0.0    5.9 3 ; dih   CCA  CBZ  CBY  CBX
  62  61  60  59   1      0.0    5.9 3      0.0    5.9 3 ; dih   CCB  CCA  CBZ  CBY
  63  62  61  60   1      0.0    5.9 3      0.0    5.9 3 ; dih   CCC  CCB  CCA  CBZ
  64  63  62  61   1      0.0    5.9 3      0.0    5.9 3 ; dih   CCD  CCC  CCB  CCA
  65  64  63  62   1      0.0    5.9 3      0.0    5.9 3 ; dih   CCE  CCD  CCC  CCB
  66  65  64  63   1      0.0    5.9 3      0.0    5.9 3 ; dih   CCF  CCE  CCD  CCC
  67  66  65  64   1      0.0    5.9 3      0.0    5.9 3 ; dih   CCG  CCF  CCE  CCD
  68  67  66  65   1      0.0    5.9 3      0.0    5.9 3 ; dih   CCH  CCG  CCF  CCE
```

```
  69   68   67   66    1       0.0     5.9 3       0.0     5.9 3 ; dih   CCI  CCH  CCG  CCF
  70   69   68   67    1       0.0     5.9 3       0.0     5.9 3 ; dih   CCJ  CCI  CCH  CCG
  71   70   69   68    1       0.0     5.9 3       0.0     5.9 3 ; dih   CCK  CCJ  CCI  CCH
```

Table S2: bodipy.itp

```
[ moleculetype ]
; Name nrexcl
_2        3

[ atoms ]
;   nr       type  resnr resid  atom  cgnr    charge      mass
     1        CH3      1  _2       CBM     1    0.000  15.0350
     2        CH2      1  _2       CBL     2    0.000  14.0270
     3        CH2      1  _2       CBK     3    0.000  14.0270
     4        CH2      1  _2       CBJ     4    0.000  14.0270
     5        CH2      1  _2       CBI     5    0.000  14.0270
     6        CH2      1  _2       CBH     6    0.000  14.0270
     7        CH2      1  _2       CBG     7    0.000  14.0270
     8        CH2      1  _2       CBF     8    0.000  14.0270
     9        CH2      1  _2       CBE     9    0.000  14.0270
    10        CH2      1  _2       CBD    10    0.000  14.0270
    11        CH2      1  _2       CBC    11    0.000  14.0270
    12        CH2      1  _2       CBB    12    0.000  14.0270
    13        CH2      1  _2       CBA    13    0.000  14.0270
    14        CH2      1  _2       CAZ    14    0.000  14.0270
    15        CH2      1  _2       CAY    15    0.000  14.0270
    16        CH2      1  _2       CAX    16    0.000  14.0270
    17        CH2      1  _2       CAW    17    0.000  14.0270
    18        CH2      1  _2       CAV    18    0.000  14.0270
    19          C      1  _2       CAH    19    0.280  12.0110
    20        CR1      1  _2       CAG    19   -0.311  12.0110
    21         HC      1  _2       HAG    19    0.170   1.0080
    22        CR1      1  _2       CAF    19   -0.242  12.0110
    23         HC      1  _2       HAF    19    0.182   1.0080
    24          C      1  _2       CAJ    19    0.044  12.0110
    25          C      1  _2       CAK    20    0.134  12.0110
    26          N      1  _2       NAO    20   -0.413  14.0067
    27          H      1  _2       HAO    20    0.287   1.0080
    28        CH2      1  _2       CAP    20    0.369  14.0270
    29        CH2      1  _2       CAQ    21   -0.106  14.0270
    30      SDMSO      1  _2       SAR    21    0.945  32.0600
    31         OM      1  _2       OAT    21   -0.613  15.9994   ; ODmso ?
    32         OM      1  _2       OAU    21   -0.613  15.9994   ; ODmso ?
    33         OM      1  _2       OAS    21   -0.613  15.9994   ; ODmso ?
    34         NR      1  _2       NAI    22   -0.179  14.0067
    35          B      1  _2       BAL    22    0.494  10.8110   ; boron
    36          F      1  _2       FAM    22   -0.354  18.9984
    37          F      1  _2       FAN    22   -0.354  18.9984
    38         NR      1  _2       NAE    22   -0.179  14.0067
    39          C      1  _2       CAC    23    0.044  12.0110
    40        CR1      1  _2       CAB    23   -0.242  12.0110
    41         HC      1  _2       HAB    23    0.182   1.0080
    42        CR1      1  _2       CAA    23   -0.311  12.0110
    43         HC      1  _2       HAA    23    0.170   1.0080
    44          C      1  _2       CAD    23    0.229  12.0110
    45        CH2      1  _2       CBN    24    0.000  14.0270
    46        CH2      1  _2       CBO    25    0.000  14.0270
    47        CH2      1  _2       CBP    26    0.000  14.0270
    48        CH2      1  _2       CBQ    27    0.000  14.0270
    49        CH2      1  _2       CBR    28    0.000  14.0270
    50        CH2      1  _2       CBS    29    0.000  14.0270
    51        CH2      1  _2       CBT    30    0.000  14.0270
```

```
    52       CH2     1   _2      CBU    31    0.000  14.0270
    53       CH2     1   _2      CBV    32    0.000  14.0270
    54       CH2     1   _2      CBW    33    0.000  14.0270
    55       CH2     1   _2      CBX    34    0.000  14.0270
    56       CH2     1   _2      CBY    35    0.000  14.0270
    57       CH2     1   _2      CBZ    36    0.000  14.0270
    58       CH2     1   _2      CCA    37    0.000  14.0270
    59       CH2     1   _2      CCB    38    0.000  14.0270
    60       CH2     1   _2      CCC    39    0.000  14.0270
    61       CH2     1   _2      CCD    40    0.000  14.0270
    62       CH3     1   _2      CCE    41    0.000  15.0350

[ bonds ]
; ai  aj  fu    c0, c1, ...
   2   1   2    0.153   7150000.0    0.153   7150000.0 ;   CBL  CBM
   2   3   2    0.153   7150000.0    0.153   7150000.0 ;   CBL  CBK
   3   4   2    0.153   7150000.0    0.153   7150000.0 ;   CBK  CBJ
   4   5   2    0.153   7150000.0    0.153   7150000.0 ;   CBJ  CBI
   5   6   2    0.153   7150000.0    0.153   7150000.0 ;   CBI  CBH
   6   7   2    0.153   7150000.0    0.153   7150000.0 ;   CBH  CBG
   7   8   2    0.153   7150000.0    0.153   7150000.0 ;   CBG  CBF
   8   9   2    0.153   7150000.0    0.153   7150000.0 ;   CBF  CBE
   9  10   2    0.153   7150000.0    0.153   7150000.0 ;   CBE  CBD
  10  11   2    0.153   7150000.0    0.153   7150000.0 ;   CBD  CBC
  11  12   2    0.153   7150000.0    0.153   7150000.0 ;   CBC  CBB
  12  13   2    0.153   7150000.0    0.153   7150000.0 ;   CBB  CBA
  13  14   2    0.153   7150000.0    0.153   7150000.0 ;   CBA  CAZ
  14  15   2    0.153   7150000.0    0.153   7150000.0 ;   CAZ  CAY
  15  16   2    0.153   7150000.0    0.153   7150000.0 ;   CAY  CAX
  16  17   2    0.153   7150000.0    0.153   7150000.0 ;   CAX  CAW
  17  18   2    0.153   7150000.0    0.153   7150000.0 ;   CAW  CAV
  19  18   2    0.153   7150000.0    0.153   7150000.0 ;   CAH  CAV
  19  20   2    0.133  11800000.0    0.133  11800000.0 ;   CAH  CAG
  19  34   2    0.133  11800000.0    0.133  11800000.0 ;   CAH  NAI
  20  21   2    0.109  12300000.0    0.109  12300000.0 ;   CAG  HAG
  20  22   2    0.133  11800000.0    0.133  11800000.0 ;   CAG  CAF
  22  23   2    0.109  12300000.0    0.109  12300000.0 ;   CAF  HAF
  24  22   2    0.133  11800000.0    0.133  11800000.0 ;   CAJ  CAF
  24  25   2    0.133  11800000.0    0.133  11800000.0 ;   CAJ  CAK
  24  34   2    0.133  11800000.0    0.133  11800000.0 ;   CAJ  NAI
  25  26   2    0.133  10600000.0    0.133  10600000.0 ;   CAK  NAO
  26  27   2    0.100  18700000.0    0.100  18700000.0 ;   NAO  HAO
  25  39   2    0.133  11800000.0    0.133  11800000.0 ;   CAK  CAC
  28  26   2    0.147   8710000.0    0.147   8710000.0 ;   CAP  NAO
  28  29   2    0.153   7150000.0    0.153   7150000.0 ;   CAP  CAQ
  30  29   2    0.183   5620000.0    0.183   5620000.0 ;   SAR  CAQ
  30  31   2    0.153   8040000.0    0.153   8040000.0 ;   SAR  OAT
  30  32   2    0.153   8040000.0    0.153   8040000.0 ;   SAR  OAU
  30  33   2    0.153   8040000.0    0.153   8040000.0 ;   SAR  OAS
  35  34   2    0.155    291912.0    0.155    291912.0 ;   BAL  NAI   B-N OK
  35  36   2    0.139    453246.0    0.139    453246.0 ;   BAL  FAM   B-F OK
  35  37   2    0.139    453246.0    0.153    453246.0 ;   BAL  FAN   B-F OK
  35  38   2    0.155    291912.0    0.155    291912.0 ;   BAL  NAE   B-N OK
  38  39   2    0.133  11800000.0    0.133  11800000.0 ;   NAE  CAC
  38  44   2    0.133  11800000.0    0.133  11800000.0 ;   NAE  CAD
  39  40   2    0.133  11800000.0    0.133  11800000.0 ;   CAC  CAB
  40  41   2    0.109  12300000.0    0.109  12300000.0 ;   CAB  HAB
  40  42   2    0.133  11800000.0    0.133  11800000.0 ;   CAB  CAA
  42  43   2    0.109  12300000.0    0.109  12300000.0 ;   CAA  HAA
  44  42   2    0.133  11800000.0    0.133  11800000.0 ;   CAD  CAA
  44  45   2    0.153   7150000.0    0.153   7150000.0 ;   CAD  CBN
  45  46   2    0.153   7150000.0    0.153   7150000.0 ;   CBN  CBO
  46  47   2    0.153   7150000.0    0.153   7150000.0 ;   CBO  CBP
  47  48   2    0.153   7150000.0    0.153   7150000.0 ;   CBP  CBQ
  48  49   2    0.153   7150000.0    0.153   7150000.0 ;   CBQ  CBR
  49  50   2    0.153   7150000.0    0.153   7150000.0 ;   CBR  CBS
  50  51   2    0.153   7150000.0    0.153   7150000.0 ;   CBS  CBT
  51  52   2    0.153   7150000.0    0.153   7150000.0 ;   CBT  CBU
  52  53   2    0.153   7150000.0    0.153   7150000.0 ;   CBU  CBV
```

```
  53  54   2    0.153   7150000.0    0.153   7150000.0 ;   CBV  CBW
  54  55   2    0.153   7150000.0    0.153   7150000.0 ;   CBW  CBX
  55  56   2    0.153   7150000.0    0.153   7150000.0 ;   CBX  CBY
  56  57   2    0.153   7150000.0    0.153   7150000.0 ;   CBY  CBZ
  57  58   2    0.153   7150000.0    0.153   7150000.0 ;   CBZ  CCA
  58  59   2    0.153   7150000.0    0.153   7150000.0 ;   CCA  CCB
  59  60   2    0.153   7150000.0    0.153   7150000.0 ;   CCB  CCC
  60  61   2    0.153   7150000.0    0.153   7150000.0 ;   CCC  CCD
  61  62   2    0.153   7150000.0    0.153   7150000.0 ;   CCD  CCE

[ pairs ]
; ai  aj  fu    c0, c1, ...
   1   4   1                                            ;   CBM  CBJ
   2   5   1                                            ;   CBL  CBI
   3   6   1                                            ;   CBK  CBH
   4   7   1                                            ;   CBJ  CBG
   5   8   1                                            ;   CBI  CBF
   6   9   1                                            ;   CBH  CBE
   7  10   1                                            ;   CBG  CBD
   8  11   1                                            ;   CBF  CBC
   9  12   1                                            ;   CBE  CBB
  10  13   1                                            ;   CBD  CBA
  11  14   1                                            ;   CBC  CAZ
  12  15   1                                            ;   CBB  CAY
  13  16   1                                            ;   CBA  CAX
  14  17   1                                            ;   CAZ  CAW
  15  18   1                                            ;   CAY  CAV
  16  19   1                                            ;   CAX  CAH
  17  20   1                                            ;   CAW  CAG
  17  34   1                                            ;   CAW  NAI
  18  21   1                                            ;   CAV  HAG
  18  22   1                                            ;   CAV  CAF
  18  24   1                                            ;   CAV  CAJ
  18  35   1                                            ;   CAV  BAL
  19  23   1                                            ;   CAH  HAF
  19  25   1                                            ;   CAH  CAK
  19  36   1                                            ;   CAH  FAM
  19  37   1                                            ;   CAH  FAN
  19  38   1                                            ;   CAH  NAE
  20  25   1                                            ;   CAG  CAK
  20  35   1                                            ;   CAG  BAL
  21  23   1                                            ;   HAG  HAF
  21  24   1                                            ;   HAG  CAJ
  21  34   1                                            ;   HAG  NAI
  22  26   1                                            ;   CAF  NAO
  22  35   1                                            ;   CAF  BAL
  22  39   1                                            ;   CAF  CAC
  23  25   1                                            ;   HAF  CAK
  23  34   1                                            ;   HAF  NAI
  24  28   1                                            ;   CAJ  CAP
  24  36   1                                            ;   CAJ  FAM
  24  37   1                                            ;   CAJ  FAN
  24  38   1                                            ;   CAJ  NAE
  24  40   1                                            ;   CAJ  CAB
  25  29   1                                            ;   CAK  CAQ
  25  35   1                                            ;   CAK  BAL
  25  41   1                                            ;   CAK  HAB
  25  42   1                                            ;   CAK  CAA
  25  44   1                                            ;   CAK  CAD
  26  30   1                                            ;   NAO  SAR
  26  34   1                                            ;   NAO  NAI
  26  38   1                                            ;   NAO  NAE
  26  40   1                                            ;   NAO  CAB
  27  29   1                                            ;   HAO  CAQ added manually
  27  24   1                                            ;   HAO  CAJ added manually
  27  39   1                                            ;   HAO  CAC added manually
  28  31   1                                            ;   CAP  OAT
  28  32   1                                            ;   CAP  OAU
  28  34   1                                            ;   CAP  OAS
```

```
  28  39   1                                          ;   CAP  CAC
  34  39   1                                          ;   NAI  CAC
  34  44   1                                          ;   NAI  CAD
  35  40   1                                          ;   BAL  CAB
  35  42   1                                          ;   BAL  CAA
  35  45   1                                          ;   BAL  CBN
  36  39   1                                          ;   FAM  CAC
  36  44   1                                          ;   FAM  CAD
  37  39   1                                          ;   FAN  CAC
  37  44   1                                          ;   FAN  CAD
  38  41   1                                          ;   NAE  HAB
  38  43   1                                          ;   NAE  HAA
  38  46   1                                          ;   NAE  CBO
  39  43   1                                          ;   CAC  HAA
  39  45   1                                          ;   CAC  CBN
  40  45   1                                          ;   CAB  CBN
  41  43   1                                          ;   HAB  HAA
  41  44   1                                          ;   HAB  CAD
  42  46   1                                          ;   CAA  CBO
  43  45   1                                          ;   HAA  CBN
  44  47   1                                          ;   CAD  CBP
  45  48   1                                          ;   CBN  CBQ
  46  49   1                                          ;   CBO  CBR
  47  50   1                                          ;   CBP  CBS
  48  51   1                                          ;   CBQ  CBT
  49  52   1                                          ;   CBR  CBU
  50  53   1                                          ;   CBS  CBV
  51  54   1                                          ;   CBT  CBW
  52  55   1                                          ;   CBU  CBX
  53  56   1                                          ;   CBV  CBY
  54  57   1                                          ;   CBW  CBZ
  55  58   1                                          ;   CBX  CCA
  56  59   1                                          ;   CBY  CCB
  57  60   1                                          ;   CBZ  CCC
  58  61   1                                          ;   CCA  CCD
  59  62   1                                          ;   CCB  CCE

[ angles ]
; ai  aj  ak  fu    c0, c1, ...
   1   2   3   2    109.5       520.0    109.5       520.0 ;   CBM  CBL  CBK
   2   3   4   2    109.5       520.0    109.5       520.0 ;   CBL  CBK  CBJ
   3   4   5   2    109.5       520.0    109.5       520.0 ;   CBK  CBJ  CBI
   4   5   6   2    109.5       520.0    109.5       520.0 ;   CBJ  CBI  CBH
   5   6   7   2    109.5       520.0    109.5       520.0 ;   CBI  CBH  CBG
   6   7   8   2    109.5       520.0    109.5       520.0 ;   CBH  CBG  CBF
   7   8   9   2    109.5       520.0    109.5       520.0 ;   CBG  CBF  CBE
   8   9  10   2    109.5       520.0    109.5       520.0 ;   CBF  CBE  CBD
   9  10  11   2    109.5       520.0    109.5       520.0 ;   CBE  CBD  CBC
  10  11  12   2    109.5       520.0    109.5       520.0 ;   CBD  CBC  CBB
  11  12  13   2    109.5       520.0    109.5       520.0 ;   CBC  CBB  CBA
  12  13  14   2    109.5       520.0    109.5       520.0 ;   CBB  CBA  CAZ
  13  14  15   2    109.5       520.0    109.5       520.0 ;   CBA  CAZ  CAY
  14  15  16   2    109.5       520.0    109.5       520.0 ;   CAZ  CAY  CAX
  15  16  17   2    109.5       520.0    109.5       520.0 ;   CAY  CAX  CAW
  16  17  18   2    109.5       520.0    109.5       520.0 ;   CAX  CAW  CAV
  17  18  19   2    109.5       520.0    109.5       520.0 ;   CAW  CAV  CAH
  18  19  20   2    120.0       560.0    120.0       560.0 ;   CAV  CAH  CAG
  18  19  34   2    120.0       560.0    120.0       560.0 ;   CAV  CAH  NAI
  20  19  34   2    108.0       465.0    108.0       465.0 ;   CAG  CAH  NAI
  19  20  21   2    126.0       575.0    126.0       575.0 ;   CAH  CAG  HAG
  19  20  22   2    108.0       465.0    108.0       465.0 ;   CAH  CAG  CAF
  21  20  22   2    126.0       575.0    126.0       575.0 ;   HAG  CAG  CAF
  20  22  23   2    126.0       575.0    126.0       575.0 ;   CAG  CAF  HAF
  20  22  24   2    108.0       465.0    108.0       465.0 ;   CAG  CAF  CAJ
  23  22  24   2    126.0       575.0    126.0       575.0 ;   HAF  CAF  CAJ
  22  24  25   2    132.0       760.0    132.0       760.0 ;   CAF  CAJ  CAK
  22  24  34   2    108.0       465.0    108.0       465.0 ;   CAF  CAJ  NAI
  25  24  34   2    120.0       560.0    120.0       560.0 ;   CAK  CAJ  NAI
  24  25  26   2    115.0       610.0    115.0       610.0 ;   CAJ  CAK  NAO
```

```
  24  25  39   2    120.0       560.0    120.0       560.0 ;   CAJ  CAK  CAC
  26  25  39   2    115.0       610.0    115.0       610.0 ;   NAO  CAK  CAC
  25  26  28   2    128.9       700.0    128.9       700.0 ;   CAK  NAO  CAP ga_30
modified to 128.9Â°
  26  28  29   2    109.5       520.0    109.5       520.0 ;   NAO  CAP  CAQ
  27  26  25   2    115.8       415.0    115.8       415.0 ;   HAO  NAO  CAK ga_31
modified to 115.8Â°
  27  26  28   2    115.3       460.0    115.3       460.0 ;   HAO  NAO  CAP ga_17
modified to 115.3Â°
  28  29  30   2    109.5       520.0    109.5       520.0 ;   CAP  CAQ  SAR
  29  30  31   2    109.5       518.0    109.5       518.0 ;   CAQ  SAR  OAT
  29  30  32   2    109.5       518.0    109.5       518.0 ;   CAQ  SAR  OAU
  29  30  33   2    109.5       518.0    109.5       518.0 ;   CAQ  SAR  OAS
  31  30  32   2    109.5       518.0    109.5       518.0 ;   OAT  SAR  OAU
  31  30  33   2    109.5       518.0    109.5       518.0 ;   OAT  SAR  OAS
  32  30  33   2    109.5       518.0    109.5       518.0 ;   OAU  SAR  OAS
  19  34  24   2    108.0       465.0    108.0       465.0 ;   CAH  NAI  CAJ
  19  34  35   2    125.0       375.0    125.0       375.0 ;   CAH  NAI  BAL   C-N-B C
  24  34  35   2    125.0       375.0    125.0       375.0 ;   CAJ  NAI  BAL   C-N-B C
  34  35  36   2    110.1       696.4    110.1       696.4 ;   NAI  BAL  FAM   N-B-F
OK
  34  35  37   2    110.1       696.4    110.1       696.4 ;   NAI  BAL  FAN   N-B-F
OK
  34  35  38   2    109.5       447.3    109.5       447.3 ;   NAI  BAL  NAE   N-B-N C
  36  35  37   2    110.7       788.2    110.7       788.2 ;   FAM  BAL  FAN   F-B-F
OK
  36  35  38   2    110.1       696.4    110.1       696.4 ;   FAM  BAL  NAE   F-B-N
OK
  37  35  38   2    110.1       696.4    110.1       696.4 ;   FAN  BAL  NAE   F-B-N
OK
  35  38  39   2    125.0       375.0    125.0       375.0 ;   BAL  NAE  CAC   B-N-C C
  35  38  44   2    125.0       375.0    125.0       375.0 ;   BAL  NAE  CAD   B-N-C C
  39  38  44   2    108.0       465.0    108.0       465.0 ;   CAC  NAE  CAD
  25  39  38   2    120.0       560.0    120.0       560.0 ;   CAK  CAC  NAE
  25  39  40   2    132.0       760.0    132.0       760.0 ;   CAK  CAC  CAB
  38  39  40   2    108.0       465.0    108.0       465.0 ;   NAE  CAC  CAB
  39  40  41   2    126.0       575.0    126.0       575.0 ;   CAC  CAB  HAB
  39  40  42   2    108.0       465.0    108.0       465.0 ;   CAC  CAB  CAA
  41  40  42   2    126.0       575.0    126.0       575.0 ;   HAB  CAB  CAA
  40  42  43   2    126.0       575.0    126.0       575.0 ;   CAB  CAA  HAA
  40  42  44   2    108.0       465.0    108.0       465.0 ;   CAB  CAA  CAD
  43  42  44   2    126.0       575.0    126.0       575.0 ;   HAA  CAA  CAD
  38  44  42   2    108.0       465.0    108.0       465.0 ;   NAE  CAD  CAA
  38  44  45   2    120.0       560.0    120.0       560.0 ;   NAE  CAD  CBN
  42  44  45   2    120.0       560.0    120.0       560.0 ;   CAA  CAD  CBN
  44  45  46   2    109.5       520.0    109.5       520.0 ;   CAD  CBN  CBO
  45  46  47   2    109.5       520.0    109.5       520.0 ;   CBN  CBO  CBP
  46  47  48   2    109.5       520.0    109.5       520.0 ;   CBO  CBP  CBQ
  47  48  49   2    109.5       520.0    109.5       520.0 ;   CBP  CBQ  CBR
  48  49  50   2    109.5       520.0    109.5       520.0 ;   CBQ  CBR  CBS
  49  50  51   2    109.5       520.0    109.5       520.0 ;   CBR  CBS  CBT
  50  51  52   2    109.5       520.0    109.5       520.0 ;   CBS  CBT  CBU
  51  52  53   2    109.5       520.0    109.5       520.0 ;   CBT  CBU  CBV
  52  53  54   2    109.5       520.0    109.5       520.0 ;   CBU  CBV  CBW
  53  54  55   2    109.5       520.0    109.5       520.0 ;   CBV  CBW  CBX
  54  55  56   2    109.5       520.0    109.5       520.0 ;   CBW  CBX  CBY
  55  56  57   2    109.5       520.0    109.5       520.0 ;   CBX  CBY  CBZ
  56  57  58   2    109.5       520.0    109.5       520.0 ;   CBY  CBZ  CCA
  57  58  59   2    109.5       520.0    109.5       520.0 ;   CBZ  CCA  CCB
  58  59  60   2    109.5       520.0    109.5       520.0 ;   CCA  CCB  CCC
  59  60  61   2    109.5       520.0    109.5       520.0 ;   CCB  CCC  CCD
  60  61  62   2    109.5       520.0    109.5       520.0 ;   CCC  CCD  CCE

[ dihedrals ]
; ai  aj  ak  al  fu    c0, c1, m, ...
  19  18  34  20   2      0.0  167.4       0.0  167.4   ; imp   CAH  CAV  NAI  CAG
  20  19  22  21   2      0.0  167.4       0.0  167.4   ; imp   CAG  CAH  CAF  HAG
  22  20  24  23   2      0.0  167.4       0.0  167.4   ; imp   CAF  CAG  CAJ  HAF
  24  34  25  22   2      0.0  167.4       0.0  167.4   ; imp   CAJ  NAI  CAK  CAF
```

```
  25  39  26  24   2      0.0  167.4        0.0  167.4   ; imp   CAK  CAC  NAO  CAJ
  30  29  32  31   2     35.3  334.8       35.3  334.8   ; imp   SAR  CAQ  OAU  OAT
  34  35  24  19   2      0.0  167.4        0.0  167.4   ; imp   NAI  BAL  CAJ  CAH
  24  34  38  35   2    180.0   46.2      180.0   46.2   ; imp   CAJ  NAI  NAE  BAL
custom for boron
  39  34  38  35   2    180.0   46.2      180.0   46.2   ; imp   CAJ  NAI  NAE  BAL
custom for boron
  35  34  36  37   2     35.3  334.8       35.3  334.8   ; imp   BAL  NAI  FAM  FAN
  38  35  44  39   2      0.0  167.4        0.0  167.4   ; imp   NAE  BAL  CAD  CAC
  39  25  38  40   2      0.0  167.4        0.0  167.4   ; imp   CAC  CAK  NAE  CAB
  40  39  42  41   2      0.0  167.4        0.0  167.4   ; imp   CAB  CAC  CAA  HAB
  42  40  44  43   2      0.0  167.4        0.0  167.4   ; imp   CAA  CAB  CAD  HAA
  44  38  45  42   2      0.0  167.4        0.0  167.4   ; imp   CAD  NAE  CBN  CAA
  19  20  22  24   2      0.0  209.3        0.0  209.3   ; imp   CAH  CAG  CAF  CAJ
  20  22  24  34   2      0.0  209.3        0.0  209.3   ; imp   CAG  CAF  CAJ  NAI
  22  24  34  19   2      0.0  209.3        0.0  209.3   ; imp   CAF  CAJ  NAI  CAH
  24  34  19  20   2      0.0  209.3        0.0  209.3   ; imp   CAJ  NAI  CAH  CAG
  34  19  20  22   2      0.0  209.3        0.0  209.3   ; imp   NAI  CAH  CAG  CAF
  38  39  40  42   2      0.0  209.3        0.0  209.3   ; imp   NAE  CAC  CAB  CAA
  39  40  42  44   2      0.0  209.3        0.0  209.3   ; imp   CAC  CAB  CAA  CAD
  40  42  44  38   2      0.0  209.3        0.0  209.3   ; imp   CAB  CAA  CAD  NAE
  42  44  38  39   2      0.0  209.3        0.0  209.3   ; imp   CAA  CAD  NAE  CAC
  44  38  39  40   2      0.0  209.3        0.0  209.3   ; imp   CAD  NAE  CAC  CAB
   4   3   2   1   1      0.0    5.9 3      0.0    5.9 3 ; dih   CBJ  CBK  CBL  CBM
   5   4   3   2   1      0.0    5.9 3      0.0    5.9 3 ; dih   CBI  CBJ  CBK  CBL
   6   5   4   3   1      0.0    5.9 3      0.0    5.9 3 ; dih   CBH  CBI  CBJ  CBK
   7   6   5   4   1      0.0    5.9 3      0.0    5.9 3 ; dih   CBG  CBH  CBI  CBJ
   8   7   6   5   1      0.0    5.9 3      0.0    5.9 3 ; dih   CBF  CBG  CBH  CBI
   9   8   7   6   1      0.0    5.9 3      0.0    5.9 3 ; dih   CBE  CBF  CBG  CBH
  10   9   8   7   1      0.0    5.9 3      0.0    5.9 3 ; dih   CBD  CBE  CBF  CBG
  11  10   9   8   1      0.0    5.9 3      0.0    5.9 3 ; dih   CBC  CBD  CBE  CBF
  12  11  10   9   1      0.0    5.9 3      0.0    5.9 3 ; dih   CBB  CBC  CBD  CBE
  13  12  11  10   1      0.0    5.9 3      0.0    5.9 3 ; dih   CBA  CBB  CBC  CBD
  14  13  12  11   1      0.0    5.9 3      0.0    5.9 3 ; dih   CAZ  CBA  CBB  CBC
  15  14  13  12   1      0.0    5.9 3      0.0    5.9 3 ; dih   CAY  CAZ  CBA  CBB
  16  15  14  13   1      0.0    5.9 3      0.0    5.9 3 ; dih   CAX  CAY  CAZ  CBA
  17  16  15  14   1      0.0    5.9 3      0.0    5.9 3 ; dih   CAW  CAX  CAY  CAZ
  18  17  16  15   1      0.0    5.9 3      0.0    5.9 3 ; dih   CAV  CAW  CAX  CAY
  19  18  17  16   1      0.0    5.9 3      0.0    5.9 3 ; dih   CAH  CAV  CAW  CAX
  17  18  19  34   1      0.0    1.0 6      0.0    1.0 6 ; dih   CAW  CAV  CAH  NAI
  39  25  24  22   1    180.0   33.5 2    180.0   33.5 2 ; dih   CAC  CAK  CAJ  CAF
set as double bond to be planar
  26  25  24  22   1    180.0   33.5 2    180.0   33.5 2 ; dih   CAC  CAK  CAJ  CAF
set as double bond to be planar
  24  25  26  28   1    180.0   33.5 2    180.0   33.5 2 ; dih   CAJ  CAK  NAO  CAP
180Â° angle between NHR and aromatic cycle.
  24  25  26  27   1    180.0   33.5 2    180.0   33.5 2 : dih   CAJ  CAK  NAO  HAO
180Â° angle between NHR and aromatic cycle.
  40  39  25  26   1    180.0   33.5 2    180.0   33.5 2 ; dih   CAB  CAC  CAK  NAO
set as double bond to be planar
  29  28  26  25   1    180.0    1.0 6    180.0    1.0 6 ; dih   CAQ  CAP  NAO  CAK
  30  29  28  26   1      0.0    5.9 3      0.0    5.9 3 ; dih   SAR  CAQ  CAP  NAO
  28  29  30  33   1      0.0    2.9 3      0.0    2.9 3 ; dih   CAP  CAQ  SAR  OAS
  38  35  34  19   1      0.0    1.0 6      0.0    1.0 6 ; dih   NAE  BAL  NAI  CAH
  34  35  38  44   1      0.0    1.0 6      0.0    1.0 6 ; dih   NAI  BAL  NAE  CAD
  46  45  44  38   1      0.0    1.0 6      0.0    1.0 6 ; dih   CBO  CBN  CAD  NAE
  47  46  45  44   1      0.0    5.9 3      0.0    5.9 3 ; dih   CBP  CBO  CBN  CAD
  48  47  46  45   1      0.0    5.9 3      0.0    5.9 3 ; dih   CBQ  CBP  CBO  CBN
  49  48  47  46   1      0.0    5.9 3      0.0    5.9 3 ; dih   CBR  CBQ  CBP  CBO
  50  49  48  47   1      0.0    5.9 3      0.0    5.9 3 ; dih   CBS  CBR  CBQ  CBP
  51  50  49  48   1      0.0    5.9 3      0.0    5.9 3 ; dih   CBT  CBS  CBR  CBQ
  52  51  50  49   1      0.0    5.9 3      0.0    5.9 3 ; dih   CBU  CBT  CBS  CBR
  53  52  51  50   1      0.0    5.9 3      0.0    5.9 3 ; dih   CBV  CBU  CBT  CBS
  54  53  52  51   1      0.0    5.9 3      0.0    5.9 3 ; dih   CBW  CBV  CBU  CBT
  55  54  53  52   1      0.0    5.9 3      0.0    5.9 3 ; dih   CBX  CBW  CBV  CBU
  56  55  54  53   1      0.0    5.9 3      0.0    5.9 3 ; dih   CBY  CBX  CBW  CBV
  57  56  55  54   1      0.0    5.9 3      0.0    5.9 3 ; dih   CBZ  CBY  CBX  CBW
  58  57  56  55   1      0.0    5.9 3      0.0    5.9 3 ; dih   CCA  CBZ  CBY  CBX
  59  58  57  56   1      0.0    5.9 3      0.0    5.9 3 ; dih   CCB  CCA  CBZ  CBY
```

```
60   59   58   57    1       0.0     5.9 3       0.0     5.9 3 ; dih    CCC   CCB   CCA   CBZ
61   60   59   58    1       0.0     5.9 3       0.0     5.9 3 ; dih    CCD   CCC   CCB   CCA
62   61   60   59    1       0.0     5.9 3       0.0     5.9 3 ; dih    CCE   CCD   CCC   CCB
```